7-2024

Adan: Adaptive Nesterov Momentum Algorithm for faster optimizing deep models

Xingyu XIE

Pan ZHOU
Singapore Management University, panzhou@smu.edu.sg

Huan LI

Zhouchen LIN

Shuicheng YAN

Citation

XIE, Xingyu; ZHOU, Pan; LI, Huan; LIN, Zhouchen; and YAN, Shuicheng. Adan: Adaptive Nesterov Momentum Algorithm for faster optimizing deep models. (2024). *IEEE Transactions on Pattern Analysis and Machine Intelligence*. 1-34.
Available at: https://ink.library.smu.edu.sg/sis_research/9037

Adan: Adaptive Nesterov Momentum Algorithm for Faster Optimizing Deep Models

Xingyu Xie[1,2*] **Pan Zhou**[1*] **Huan Li**[3] **Zhouchen Lin**[2] **Shuicheng Yan**[1]
[1]Sea AI Lab [2]Peking University [3]Nankai University
{xyxie,zhoupan,yansc}@sea.com {xyxie,zlin}@pku.cn lihuanss@nankai.edu.cn

Abstract

In deep learning, different kinds of deep networks typically need different optimizers, which have to be chosen after multiple trials, making the training process inefficient. To relieve this issue and consistently improve the model training speed across deep networks, we propose the ADAptive Nesterov momentum algorithm, Adan for short. Adan first reformulates the vanilla Nesterov acceleration to develop a new Nesterov momentum estimation (NME) method, which avoids the extra overhead of computing gradient at the extrapolation point. Then Adan adopts NME to estimate the gradient's first- and second-order moments in adaptive gradient algorithms for convergence acceleration. Besides, we prove that Adan finds an ϵ-approximate first-order stationary point within $\mathcal{O}\big(\epsilon^{-3.5}\big)$ stochastic gradient complexity on the non-convex stochastic problems (*e.g.* deep learning problems), matching the best-known lower bound. Extensive experimental results show that Adan consistently surpasses the corresponding SoTA optimizers on vision, language, and RL tasks and sets new SoTAs for many popular networks and frameworks, *e.g.* ResNet, ConvNext, ViT, Swin, MAE, DETR, GPT-2, Transformer-XL, and BERT. More surprisingly, Adan can use half of the training cost (epochs) of SoTA optimizers to achieve higher or comparable performance on ViT, GPT-2, MAE, *etc*, and also shows great tolerance to a large range of minibatch size, *e.g.* from 1k to 32k. Code is released at https://github.com/sail-sg/Adan, and has been used in multiple popular deep learning frameworks or projects.

1 Introduction

Deep neural networks (DNNs) have made remarkable success in many fields, *e.g.* computer vision [1–4] and natural language processing [5, 6]. A noticeable part of such success is contributed by the stochastic gradient-based optimizers, which find satisfactory solutions with high efficiency. Among current deep optimizers, SGD [7, 8] is the earliest and also the most representative stochastic optimizer, with dominant popularity for its simplicity and effectiveness. It adopts a single common learning rate for all gradient coordinates but often suffers unsatisfactory convergence speed on sparse data or ill-conditioned problems. In recent years, adaptive gradient algorithms [9–17] have been proposed, which adjusts the learning rate for each gradient coordinate according to the current geometry curvature of the loss objective. These adaptive algorithms often offer a faster convergence speed than SGD in practice across many DNN frameworks.

However, none of the above optimizers can always stay undefeated among all its competitors across different DNN architectures and applications. For instance, for vanilla ResNets [2], SGD often achieves better generalization performance than adaptive gradient algorithms such as Adam [18], whereas on vision transformers (ViTs) [19–21], SGD often fails, and AdamW [22] is the dominant optimizer with higher and more stable performance. Moreover, these commonly used optimizers

*Equal contribution. Xingyu did this work during an internship at Sea AI Lab.

Preprint. Under review.

Table 1: Comparison of different adaptive gradient algorithms on nonconvex stochastic problems. "Separated Reg." refers to whether the ℓ_2 regularizer (weight decay) can be separated from the loss objective like AdamW. "Complexity" denotes stochastic gradient complexity to find an ϵ-approximate first-order stationary point. Adam-type methods [31] includes Adam, AdaMomentum [32], and AdaGrad [9], AdaBound [13] and AMSGrad [11], *etc*. AdamW has no available convergence result. For SAM [33], A-NIGT [34] and Adam$^+$ [35], we compare their adaptive versions. d is the variable dimension. The lower bound is proven in [36] and please see Sec. A in Appendix for the discussion on why the lower bound is $\Omega\big(\epsilon^{-3.5}\big)$.

Smoothness Condition	Optimizer	Separated Reg.	Batch Size Condition.	Grad. Bound	Complexity	Lower Bound
Lipschitz Gradient	Adam-type [31]	✗	✗	$\ell_\infty \le c_\infty$	$\mathcal{O}\big(c_\infty^2 d\epsilon^{-4}\big)$	$\Omega\big(\epsilon^{-4}\big)$
	RMSProp [10, 37]	✗	✗	$\ell_\infty \le c_\infty$	$\mathcal{O}\big(\sqrt{c_\infty} d\epsilon^{-4}\big)$	$\Omega\big(\epsilon^{-4}\big)$
	AdamW [22]	✓	—	—	—	—
	Adabelief [15]	✗	✗	$\ell_2 \le c_2$	$\mathcal{O}\big(c_2^6 \epsilon^{-4}\big)$	$\Omega\big(\epsilon^{-4}\big)$
	Padam [38]	✗	✗	$\ell_\infty \le c_\infty$	$\mathcal{O}\big(\sqrt{c_\infty} d\epsilon^{-4}\big)$	$\Omega\big(\epsilon^{-4}\big)$
	LAMB [25]	✗	$\mathcal{O}\big(\epsilon^{-4}\big)$	$\ell_2 \le c_2$	$\mathcal{O}\big(c_2^2 d\epsilon^{-4}\big)$	$\Omega\big(\epsilon^{-4}\big)$
	Adan (ours)	✓	✗	$\ell_\infty \le c_\infty$	$\mathcal{O}\big(c_\infty^{2.5} \epsilon^{-4}\big)$	$\Omega\big(\epsilon^{-4}\big)$
Lipschitz Hessian	A-NIGT [34]	✗	✗	$\ell_2 \le c_2$	$\mathcal{O}\big(\epsilon^{-3.5} \log \frac{c_2}{\epsilon}\big)$	$\Omega\big(\epsilon^{-3.5}\big)$
	Adam$^+$ [35]	✗	$\mathcal{O}\big(\epsilon^{-1.625}\big)$	$\ell_2 \le c_2$	$\mathcal{O}\big(\epsilon^{-3.625}\big)$	$\Omega\big(\epsilon^{-3.5}\big)$
	Adan (ours)	✓	✗	$\ell_\infty \le c_\infty$	$\mathcal{O}\big(c_\infty^{1.25} \epsilon^{-3.5}\big)$	$\Omega\big(\epsilon^{-3.5}\big)$

usually fail for large-batch training, which is a default setting of the prevalent distributed training. Although there is some performance degradation, we still tend to choose the large-batch setting for large-scale deep learning training tasks due to the unaffordable training time. For example, training the ViT-B with the batch size of 512 usually takes several days, but when the batch size comes to 32K, we may finish the training within three hours [23]. Although some methods, *e.g.* LARS [24] and LAMB [25], have been proposed to handle large batch sizes, their performance may varies significantly across DNN architectures. This performance inconsistency increases the training cost and engineering burden since one has to try various optimizers for different architectures or training settings. This paper aims at relieving this issue.

When we rethink the current adaptive gradient algorithms, we find that they mainly combine the moving average idea with the heavy ball acceleration technique to estimate the first- and second-order moments of the gradient [15, 18, 22, 25]. However, previous studies [26–28] have revealed that Nesterov acceleration can theoretically achieve a faster convergence speed than heavy ball acceleration, as it uses gradient at an extrapolation point of the current solution and sees a slight "future". The ability to see the "future" may help optimizers better utilize the curve information of the dynamic training trajectory and show better robustness to DNN architectures. Moreover, recent works [29, 30] have shown the potential of Nesterov acceleration for large-batch training. Thus we are inspired to consider efficiently integrating Nesterov acceleration with adaptive algorithms.

The contributions of our work include: 1) We propose an efficient DNN optimizer, named Adan. Adan develops a Nesterov momentum estimation method to estimate stable and accurate first- and second-order moments of the gradient in adaptive gradient algorithms for acceleration. **2)** Moreover, Adan enjoys a provably faster convergence speed than previous adaptive gradient algorithms such as Adam. **3)** Empirically, Adan shows superior performance over the SoTA deep optimizers across vision, language, and reinforcement learning (RL) tasks. So it is possible that the effort on trying different optimizers for different deep network architectures can be greatly reduced. Our *detailed* contributions are highlighted below.

Firstly, we propose an efficient Nesterov-acceleration-induced deep learning optimizer termed Adan. Given a function f and the current solution $\boldsymbol{\theta}_k$, Nesterov acceleration [26–28] estimates the gradient $\mathbf{g}_k = \nabla f(\boldsymbol{\theta}'_k)$ at the extrapolation point $\boldsymbol{\theta}'_k = \boldsymbol{\theta}_k - \eta(1-\beta_1)\mathbf{m}_{k-1}$ with the learning rate η and momentum coefficient $\beta_1 \in (0,1)$, and updates the moving gradient average as $\mathbf{m}_k = (1-\beta_1)\mathbf{m}_{k-1} + \mathbf{g}_k$. Then it runs a step by $\boldsymbol{\theta}_{k+1} = \boldsymbol{\theta}_k - \eta\mathbf{m}_k$. However, the inconsistency of the positions for parameter updating at $\boldsymbol{\theta}_k$ and gradient estimation at $\boldsymbol{\theta}'_k$ leads to the additional cost of manual extrapolation and inconsistent interface with other optimizers during back-propagation (BP), which is inconvenient to use especially for large DNNs. To resolve the issues, we propose an

alternative Nesterov momentum estimation (NME). We compute the gradient $\mathbf{g}_k = \nabla f(\boldsymbol{\theta}_k)$ at the current solution $\boldsymbol{\theta}_k$, and estimate the moving gradient average as $\mathbf{m}_k = (1-\beta_1)\mathbf{m}_{k-1} + \mathbf{g}'_k$, where $\mathbf{g}'_k = \mathbf{g}_k + (1-\beta_1)(\mathbf{g}_k - \mathbf{g}_{k-1})$. Our NME is provably equivalent to the vanilla one yet can avoid the extra cost. Then by regarding $\mathbf{g}'_k$ as the current stochastic gradient in adaptive gradient algorithms, *e.g.* Adam, we accordingly estimate the first- and second-moments as $\mathbf{m}_k = (1-\beta_1)\mathbf{m}_{k-1} + \beta_1\mathbf{g}'_k$ and $\mathbf{n}_k = (1-\beta_2)\mathbf{n}_{k-1} + \beta_2(\mathbf{g}'_k)^2$, respectively. Finally, we update $\boldsymbol{\theta}_{k+1} = \boldsymbol{\theta}_k - \eta\mathbf{m}_k/(\sqrt{\mathbf{n}_k}+\varepsilon)$. In this way, Adan enjoys the merit of Nesterov acceleration, namely faster convergence speed and tolerance to large mini-batch size [39], which is verified in our experiments in Sec. 5.

Secondly, as shown in Table 1, we theoretically justify the advantages of Adan over previous SoTA adaptive gradient algorithms on nonconvex stochastic problems.

- Given the Lipschitz gradient condition, to find an ϵ-approximate first-order stationary point, Adan has the stochastic gradient complexity $\mathcal{O}\big(c_\infty^{2.5}\epsilon^{-4}\big)$ which accords with the lower bound $\Omega(\epsilon^{-4})$ (up to a constant factor) [40]. This complexity is lower than $\mathcal{O}\big(c_2^6\epsilon^{-4}\big)$ of Adabelief [15] and $\mathcal{O}\big(c_2^2 d\epsilon^{-4}\big)$ of LAMB, especially on over-parameterized networks. Specifically, for the d-dimensional gradient, compared with its ℓ_2 norm c_2, its ℓ_∞ norm c_∞ is usually much smaller, and can be $\sqrt{d}\times$ smaller for the best case. Moreover, Adan's results still hold when the loss and the ℓ_2 regularizer are separated, which could significantly benefit the generalization [19] but the convergence analysis for Adam-type optimizers remains open.
- Given the Lipschitz Hessian condition, Adan has a complexity $\mathcal{O}\big(c_\infty^{1.25}\epsilon^{-3.5}\big)$ which also matches the lower bound $\Omega(\epsilon^{-3.5})$ in [36]. This complexity is superior to $\mathcal{O}\big(\epsilon^{-3.5}\log\frac{c_2}{\epsilon}\big)$ of A-NIGT [34] and also $\mathcal{O}\big(\epsilon^{-3.625}\big)$ of Adam$^+$ [35]. Indeed, Adam$^+$ needs the minibatch size of order $\mathcal{O}\big(\epsilon^{-1.625}\big)$ which is prohibitive in practice. For other optimizers, *e.g.* Adam, their convergence has not been provided yet under the Lipschitz Hessian condition.

Finally, Adan simultaneously surpasses the corresponding SoTA optimizers across vision, language, and RL tasks, and establishes new SoTAs for many networks and settings, *e.g.* ResNet, ConvNext [4], ViT [19], Swin [20], MAE [41], LSTM [42], Transformer-XL [43], BERT [44], and GPT-2 [45]. More importantly, with half of the training cost (epochs) of SoTA optimizers, Adan can achieve higher or comparable performance on ViT, Swin, ResNet, *etc*. Besides, Adan works well in a large range of minibatch sizes, *e.g.* from 1k to 32k on ViTs. The improvement of Adan for various architectures and settings can greatly relieve the engineering burden by avoiding trying different optimizers and allowing users to accumulate consistent optimization experience.

2 Related Work

Here we mainly review deep optimizers due to limited space. Current deep optimizers can be grouped into two families: SGD and its accelerated variants, and adaptive gradient algorithms. SGD computes stochastic gradient and updates the variable along the gradient direction. Later, heavy-ball acceleration [46] movingly averages stochastic gradient in SGD for faster convergence. Nesterov acceleration [28] runs a step along the moving gradient average and then computes gradient at the new point to look ahead for correction. Typically, Nesterov acceleration converges faster both empirically and theoretically at least on convex problems, and also has superior generalization on DNNs [33, 47].

Unlike SGD, adaptive gradient algorithms, *e.g.* AdaGrad [9], RMSProp [10] and Adam, view the second momentum of gradient as a precontioner and also use moving gradient average to update the variable. Later, many variants have been proposed to estimate more accurate and stable first momentum of gradient or its second momentum, *e.g.* AMSGrad [11], Adabound [13], and Adabelief [15]. To avoid gradient collapse, AdamP [16] proposes to adaptively clip gradient. Radam [14] reduces gradient variance to stabilize training. To improve generalization, AdamW [22] splits the objective and trivial regularization, and its effectiveness is validated across many applications; SAM [33] and its variants [23, 47, 48] aim to find flat minima but need forward and backward twice per iteration. LARS [24] and LAMB [25] train DNNs with a large batch but suffer unsatisfactory performance on small batch. Padam [38] provides a simple but effective way to improve the generalization performance of Adam by adjusting the second-order moment in Adam. The most related work to ours is NAdam [49]. It simplifies Nesterov acceleration to estimating the first moment of gradient in

Adam. But its acceleration does not use any gradient from the extrapolation points and thus does not look ahead for correction. Moreover, there is no theoretical result to ensure its convergence. See more difference discussion in Sec. 3.2, especially for Eqn. (3).

3 Methodology

In this work, we study the following regularized nonconvex optimization problem:

$$\min_{\boldsymbol{\theta}} F(\boldsymbol{\theta}) \coloneqq \mathbb{E}_{\boldsymbol{\zeta}\sim\mathcal{D}}\left[f(\boldsymbol{\theta},\boldsymbol{\zeta})\right] + \frac{\lambda}{2}\|\boldsymbol{\theta}\|_2^2, \tag{1}$$

where loss $f(\cdot,\cdot)$ is differentiable and possibly nonconvex, data $\boldsymbol{\zeta}$ is drawn from an unknown distribution $\mathcal{D}$, $\boldsymbol{\theta}$ is learnable parameters, and $\|\cdot\|$ is the classical ℓ_2 norm. Here we consider the ℓ_2 regularizer as it can improve generalization performance and is widely used in practice [22]. The formulation (1) encapsulates a large body of machine learning problems, *e.g.* network training problems, and least square regression. Below, we first introduce the key motivation of Adan in Sec. 3.1, and then give detailed algorithmic steps in Sec. 3.2.

3.1 Preliminaries

Adaptive gradient algorithms, Adam [18] and AdamW [22], have become the default choice to train CNNs and ViTs. Unlike SGD which uses one learning rate for all gradient coordinates, adaptive algorithms adjust the learning rate for each gradient coordinate according to the current geometry curvature of the objective function, and thus converge faster. Take RMSProp [10] and Adam [18] as examples. Given stochastic gradient estimator $\mathbf{g}_k \coloneqq \mathbb{E}_{\boldsymbol{\zeta}\sim\mathcal{D}}[\nabla f(\boldsymbol{\theta}_k,\boldsymbol{\zeta})] + \boldsymbol{\xi}_k$, *e.g.* minibatch gradient, where $\boldsymbol{\xi}_k$ is the gradient noise, RMSProp updates the variable $\boldsymbol{\theta}$ as follows:

$$\text{RMSProp:}\begin{cases}\mathbf{n}_k = (1-\beta)\mathbf{n}_{k-1} + \beta\mathbf{g}_k^2\\ \boldsymbol{\theta}_{k+1} = \boldsymbol{\theta}_k - \boldsymbol{\eta}_k\circ\mathbf{g}_k,\end{cases}\qquad \text{Adam:}\begin{cases}\mathbf{m}_k = (1-\beta_1)\mathbf{m}_{k-1} + \beta_1\mathbf{g}_k\\ \mathbf{n}_k = (1-\beta_2)\mathbf{n}_{k-1} + \beta_2\mathbf{g}_k^2\\ \boldsymbol{\theta}_{k+1} = \boldsymbol{\theta}_k - \boldsymbol{\eta}_k\circ\mathbf{m}_k,\end{cases}$$

where $\boldsymbol{\eta}_k \coloneqq \eta/\big(\sqrt{\mathbf{n}_k}+\varepsilon\big)$, $\mathbf{m}_0=\mathbf{g}_0$, $\mathbf{n}_0=\mathbf{g}_0^2$, the scalar η is the base learning rate, $\circ$ denotes the element-wise product, and the vector square and the vector-to-vector or scalar-to-vector root in this paper are both element-wise.

Based on RMSProp, Adam (for presentation convenience, we omit the de-bias term in adaptive gradient methods), replaces the estimated gradient $\mathbf{g}_k$ with a moving average $\mathbf{m}_k$ of all previous gradient $\mathbf{g}_k$. By inspection, one can easily observe that the moving average idea in Adam is similar to the classical (stochastic) heavy-ball acceleration (HBA) technique [46]:

$$\text{HBA:}\begin{cases}\mathbf{g}_k = \nabla f(\boldsymbol{\theta}_k) + \boldsymbol{\xi}_k\\ \mathbf{m}_k = (1-\beta_1)\mathbf{m}_{k-1} + \mathbf{g}_k\\ \boldsymbol{\theta}_{k+1} = \boldsymbol{\theta}_k - \eta\mathbf{m}_k,\end{cases}\qquad \text{AGD:}\begin{cases}\mathbf{g}_k = \nabla f(\boldsymbol{\theta}_k - \eta(1-\beta_1)\mathbf{m}_{k-1}) + \boldsymbol{\xi}_k\\ \mathbf{m}_k = (1-\beta_1)\mathbf{m}_{k-1} + \mathbf{g}_k\\ \boldsymbol{\theta}_{k+1} = \boldsymbol{\theta}_k - \eta\mathbf{m}_k.\end{cases} \tag{2}$$

Both Adam and HBA share the spirit of moving gradient average, though HBA does not have the factor β_1 on the gradient $\mathbf{g}_k$. That is, given one gradient coordinate, if its gradient directions are more consistent along the optimization trajectory, Adam/HBA accumulates a larger gradient value in this direction and thus goes ahead for a bigger gradient step, which accelerates convergence.

In addition to HBA, Nesterov's accelerated (stochastic) gradient descent (AGD) [26–28] is another popular acceleration technique in the optimization community, see Eqn.(2). Unlike HBA, AGD uses the gradient at the extrapolation point $\boldsymbol{\theta}'_k = \boldsymbol{\theta}_k - \eta(1-\beta_1)\mathbf{m}_{k-1}$. Hence when the adjacent iterates share consistent gradient directions, AGD sees a slight future to converge faster. Indeed, AGD theoretically converges faster than HBA and achieves optimal convergence rate among first-order optimization methods on the general smooth convex problems [28]. It also relaxes the convergence conditions of HBA on the strongly convex problems [27]. Meanwhile, since the over-parameterized DNNs have been observed/proved to have many convex-alike local basins [50–58], AGD seems to be more suitable than HBA for DNNs. For large-batch training, [29] showed that AGD has the potential to achieve comparable performance to some specifically designed optimizers, *e.g.* LARS and LAMB. With its advantage and potential in convergence and large-batch training, we consider applying AGD to improve adaptive algorithms.

3.2 Adaptive Nesterov Momentum Algorithm

Main Iteration. We temporarily set $\lambda = 0$ in Eqn. (1). As aforementioned, AGD computes gradient at an extrapolation point $\boldsymbol{\theta}'_k$ instead of the current iterate $\boldsymbol{\theta}_k$, which however brings extra computation and memory overhead for computing $\boldsymbol{\theta}'_k$ and preserving both $\boldsymbol{\theta}_k$ and $\boldsymbol{\theta}'_k$. To solve the issue, Lemma 1 with proof in Appendix Sec. B.2 reformulates AGD (2) into its equivalent but more efficient version.

Lemma 1. *Assume $\mathbb{E}(\boldsymbol{\xi}_k) = \mathbf{0}$, $\mathrm{Cov}(\boldsymbol{\xi}_i, \boldsymbol{\xi}_j) = 0$ for any $k, i, j > 0$, $\bar{\boldsymbol{\theta}}_k$ and $\bar{\mathbf{m}}_k$ be the iterate and momentum of the vanilla AGD in Eqn. (2), respectively. Let $\boldsymbol{\theta}_{k+1} \coloneqq \bar{\boldsymbol{\theta}}_{k+1} - \eta(1-\beta_1)\bar{\mathbf{m}}_k$ and $\mathbf{m}_k \coloneqq (1-\beta_1)^2\bar{\mathbf{m}}_{k-1} + (2-\beta_1)(\nabla f(\boldsymbol{\theta}_k) + \boldsymbol{\xi}_k)$. The vanilla AGD in Eqn. (2) becomes AGD-II:*

$$\textit{AGD II:}\ \begin{cases} \mathbf{g}_k = \mathbb{E}_{\boldsymbol{\zeta}\sim\mathcal{D}}[\nabla f(\boldsymbol{\theta}_k, \boldsymbol{\zeta})] + \boldsymbol{\xi}_k \\ \mathbf{m}_k = (1-\beta_1)\mathbf{m}_{k-1} + \mathbf{g}'_k \\ \boldsymbol{\theta}_{k+1} = \boldsymbol{\theta}_k - \eta\mathbf{m}_k \end{cases},$$

where $\mathbf{g}'_k \coloneqq \mathbf{g}_k + (1-\beta_1)(\mathbf{g}_k - \mathbf{g}_{k-1})$. Moreover, if vanilla AGD in Eqn. (2) converges, so does AGD-II: $\mathbb{E}(\boldsymbol{\theta}_\infty) = \mathbb{E}(\bar{\boldsymbol{\theta}}_\infty)$.

The main idea in Lemma 1 is that we maintain $(\boldsymbol{\theta}_k - \eta(1-\beta_1)\mathbf{m}_{k-1})$ rather than $\boldsymbol{\theta}_k$ in vanilla AGD at each iteration since there is no difference between them when the algorithm converges. Like other adaptive optimizers, by regarding $\mathbf{g}'_k$ as the current stochastic gradient and movingly averaging $\mathbf{g}'_k$ to estimate the first- and second-moments of gradient, we obtain:

$$\text{Vanilla Adan:}\ \begin{cases} \mathbf{m}_k = (1-\beta_1)\mathbf{m}_{k-1} + \beta_1\mathbf{g}'_k \\ \mathbf{n}_k = (1-\beta_3)\mathbf{n}_{k-1} + \beta_3(\mathbf{g}'_k)^2 \\ \boldsymbol{\theta}_{k+1} = \boldsymbol{\theta}_k - \boldsymbol{\eta}_k \circ \mathbf{m}_k \end{cases},$$

where $\mathbf{g}'_k \coloneqq \mathbf{g}_k + (1-\beta_1)(\mathbf{g}_k - \mathbf{g}_{k-1})$ and the vector square in the second line is element-wisely. The main difference of Adan with Adam-type methods and Nadam [49] is that, as compared in Eqn. (3), the first-order moment $\mathbf{m}_k$ of Adan is the average of $\{\mathbf{g}_t + (1-\beta_1)(\mathbf{g}_t - \mathbf{g}_{t-1})\}_{t=1}^k$ while those of Adam-type and Nadam are the average of $\{\mathbf{g}_t\}_{t=1}^k$. So is their second-order term $\mathbf{n}_k$,

$$\mathbf{m}_k = \begin{cases} \sum_{t=0}^k c_{k,t}[\mathbf{g}_t + (1-\beta_1)(\mathbf{g}_t - \mathbf{g}_{t-1})], & \text{Adan,} \\ \sum_{t=0}^k c_{k,t}\mathbf{g}_t, & \text{Adam,} \\ \frac{\mu_{k+1}}{\mu'_{k+1}}\big(\sum_{t=0}^k c_{k,t}\mathbf{g}_t\big) + \frac{1-\mu_k}{\mu'_k}\mathbf{g}_k, & \text{Nadam,} \end{cases} \quad c_{k,t} = \begin{cases} \beta_1(1-\beta_1)^{k-t} & t > 0, \\ (1-\beta_1)^k & t = 0, \end{cases} \tag{3}$$

where $\{\mu_t\}_{t=1}^\infty$ is a predefined exponentially decaying sequence, $\mu'_k = 1 - \prod_{t=1}^k \mu_t$. Nadam is more like Adam than Adan, as their $\mathbf{m}_k$ averages the historical gradients instead of gradient differences in Adan. For the large k (i.e. small μ_k), $\mathbf{m}_k$ in Nadam and Adam are almost the same.

As shown in Eqn. (3), the moment $\mathbf{m}_k$ in Adan consists of two terms, i.e. gradient term $\mathbf{g}_t$ and gradient difference term $(\mathbf{g}_t - \mathbf{g}_{t-1})$, which actually have different physic meanings. So here we decouple them for greater flexibility and also better trade-off between them. Specifically, we estimate:

$$(\boldsymbol{\theta}_{k+1} - \boldsymbol{\theta}_k)/\boldsymbol{\eta}_k = \sum_{t=0}^k \big[c_{k,t}\mathbf{g}_t + (1-\beta_2)c'_{k,t}(\mathbf{g}_t - \mathbf{g}_{t-1})\big] = \mathbf{m}_k + (1-\beta_2)\mathbf{v}_k, \tag{4}$$

where $c'_{k,t} = \beta_2(1-\beta_2)^{k-t}$ for $t > 0$, $c'_{k,t} = (1-\beta_2)^k$ for $t = 0$, and and, with a little abuse of notation on $\mathbf{m}_k$, we let $\mathbf{m}_k$ and $\mathbf{v}_k$ be:

$$\mathbf{m}_k = (1-\beta_1)\mathbf{m}_{k-1} + \beta_1\mathbf{g}_k, \qquad \mathbf{v}_k = (1-\beta_2)\mathbf{v}_{k-1} + \beta_2(\mathbf{g}_k - \mathbf{g}_{k-1})$$

This change for a flexible estimation does not impair convergence speed. As shown in Theorem 1, Adan's convergence complexity still matches the best-known lower bound. We do not separate the gradients and their difference in the second-order moment $\mathbf{n}_k$, since $\mathbb{E}(\mathbf{n}_k)$ contains the correlation term $\mathrm{Cov}(\mathbf{g}_k, \mathbf{g}_{k-1}) \neq 0$ which may have statistical significance.

Decay Weight by Proximation. As observed in AdamW, decoupling the optimization objective and simple-type regularization (*e.g.* ℓ_2 regularizer) can largely improve the generalization performance.

Algorithm 1: Adan (Adaptive Nesterov Momentum Algorithm)

Input: initialization $\boldsymbol{\theta}_0$, step size η, momentum $(\beta_1, \beta_2, \beta_3) \in [0,1]^3$, stable parameter $\varepsilon > 0$, weight decay $\lambda_k > 0$, restart condition.

Output: some average of $\{\boldsymbol{\theta}_k\}_{k=1}^K$.

while $k < K$ **do**
  estimate the stochastic gradient $\mathbf{g}_k$ at $\boldsymbol{\theta}_k$;
  $\mathbf{m}_k = (1-\beta_1)\mathbf{m}_{k-1} + \beta_1 \mathbf{g}_k$;
  $\mathbf{v}_k = (1-\beta_2)\mathbf{v}_{k-1} + \beta_2(\mathbf{g}_k - \mathbf{g}_{k-1})$;
  $\mathbf{n}_k = (1-\beta_3)\mathbf{n}_{k-1} + \beta_3[\mathbf{g}_k + (1-\beta_2)(\mathbf{g}_k - \mathbf{g}_{k-1})]^2$;
  $\boldsymbol{\eta}_k = \eta / \big(\sqrt{\mathbf{n}_k} + \varepsilon\big)$;
  $\boldsymbol{\theta}_{k+1} = (1+\lambda_k \eta)^{-1}[\boldsymbol{\theta}_k - \boldsymbol{\eta}_k \circ (\mathbf{m}_k + (1-\beta_2)\mathbf{v}_k)]$;
  if *restart condition holds* **then**
    estimate stochastic gradient $\mathbf{g}_0$ at $\boldsymbol{\theta}_{k+1}$;
    set $k = 1$ and update $\boldsymbol{\theta}_1$ by Line 6;
  end if
end while

we set $\mathbf{m}_0 = \mathbf{g}_0$, $\mathbf{v}_0 = \mathbf{0}$, $\mathbf{v}_1 = \mathbf{g}_1 - \mathbf{g}_0$, and $\mathbf{n}_0 = \mathbf{g}_0^2$.

Here we follow this idea but from a rigorous optimization perspective. Intuitively, at each iteration $\boldsymbol{\theta}_{k+1} = \boldsymbol{\theta}_k - \boldsymbol{\eta}_k \circ \bar{\mathbf{m}}_k$, we minimize the first-order approximation of $F(\cdot)$ at the point $\boldsymbol{\theta}_k$:

$$\boldsymbol{\theta}_{k+1} = \operatorname*{argmin}_{\boldsymbol{\theta}} \left(F(\boldsymbol{\theta}_k) + \langle \bar{\mathbf{m}}_k, \boldsymbol{\theta} - \boldsymbol{\theta}_k \rangle + \frac{1}{2\eta} \|\boldsymbol{\theta} - \boldsymbol{\theta}_k\|^2_{\sqrt{\mathbf{n}_k}} \right),$$

where $\|\mathbf{x}\|^2_{\sqrt{\mathbf{n}_k}} := \big\langle \mathbf{x}, \big(\sqrt{\mathbf{n}_k} + \varepsilon\big) \circ \mathbf{x} \big\rangle$ and $\bar{\mathbf{m}}_k := \mathbf{m}_k + (1-\beta_2)\mathbf{v}_k$ is the first-order derivative of $F(\cdot)$ in some sense. Follow the idea of proximal gradient descent [59, 60], we decouple the ℓ_2 regularizer from $F(\cdot)$ and only linearize the loss function $f(\cdot)$:

$$\boldsymbol{\theta}_{k+1} = \operatorname*{argmin}_{\boldsymbol{\theta}} \left(F'_k(\boldsymbol{\theta}) + \langle \bar{\mathbf{m}}_k, \boldsymbol{\theta} - \boldsymbol{\theta}_k \rangle + \frac{1}{2\eta} \|\boldsymbol{\theta} - \boldsymbol{\theta}_k\|^2_{\sqrt{\mathbf{n}_k}} \right) = \frac{\boldsymbol{\theta}_k - \boldsymbol{\eta}_k \circ \bar{\mathbf{m}}_k}{1 + \lambda_k \eta}, \tag{5}$$

where $F'_k(\boldsymbol{\theta}) := \mathbb{E}_{\boldsymbol{\zeta} \sim \mathcal{D}} \left[f(\boldsymbol{\theta}_k, \boldsymbol{\zeta}) \right] + \frac{\lambda_k}{2} \|\boldsymbol{\theta}\|^2_{\sqrt{\mathbf{n}_k}}$, and $\lambda_k > 0$ is the weight decay at the k-th iteration. Interestingly, we can easily reveal the updating rule $\boldsymbol{\theta}_{k+1} = (1 - \lambda\eta)\boldsymbol{\theta}_k - \boldsymbol{\eta}_k \circ \bar{\mathbf{m}}_k$ of AdamW by using the first-order approximation of Eqn. (5) around $\eta = 0$: 1) $(1+\lambda\eta)^{-1} = (1-\lambda\eta) + \mathcal{O}\big(\eta^2\big)$; 2) $\lambda\eta\boldsymbol{\eta}_k = \mathcal{O}\big(\eta^2\big) / \big(\sqrt{\mathbf{n}_k} + \varepsilon\big)$.

One can find that the optimization objective of Separated Regularization at the k-th iteration is changed from the vanilla "static" function $F(\cdot)$ in Eqn. (1) to a "dynamic" function $F_k(\cdot)$ in Eqn. (6), which adaptively regularizes the coordinates with larger gradient more:

$$F_k(\boldsymbol{\theta}) := \mathbb{E}_{\boldsymbol{\zeta} \sim \mathcal{D}} \left[f(\boldsymbol{\theta}, \boldsymbol{\zeta}) \right] + \frac{\lambda_k}{2} \|\boldsymbol{\theta}\|^2_{\sqrt{\mathbf{n}_k}}. \tag{6}$$

We summarize our Adan in Algorithm 1. We reset the momentum term properly by the restart condition, a common trick to stabilize optimization and benefit convergence [61, 62]. But to make Adan simple, in all experiments except Table 13, we do not use this restart strategy although it can improve performance as shown in Table 13.

4 Convergence Analysis

For analysis, we make several mild assumptions used in many works, *e.g.* [15, 31–35, 37, 38, 47].

Assumption 1 (L-smoothness)**.** *The function $f(\cdot, \cdot)$ is L-smooth:*

$$\|\nabla \mathbb{E}_{\boldsymbol{\zeta}}[f(\mathbf{x}, \boldsymbol{\zeta})] - \nabla \mathbb{E}_{\boldsymbol{\zeta}}[f(\mathbf{y}, \boldsymbol{\zeta})]\| \le L\|\mathbf{x} - \mathbf{y}\|, \qquad \forall \mathbf{x},\ \mathbf{y}.$$

Assumption 2 (Unbiased and bounded gradient oracle)**.** *The stochastic gradient oracle $\mathbf{g}_k = \mathbb{E}_{\boldsymbol{\zeta}}[\nabla f(\boldsymbol{\theta}_k, \boldsymbol{\zeta})] + \boldsymbol{\xi}_k$ is unbiased, and its magnitude and variance are bounded with probability 1:*

$$\mathbb{E}\left(\boldsymbol{\xi}_k\right) = \mathbf{0}, \quad \|\mathbf{g}_k\|_\infty \le c_\infty / 3, \quad \mathbb{E}\Big(\|\boldsymbol{\xi}_k\|^2\Big) \le \sigma^2, \quad \forall k \in [T].$$

Assumption 3 (ρ-Lipschitz continuous Hessian)**.** *The function $f(\cdot,\cdot)$ has ρ-Lipschitz Hessian:*

$$\left\|\nabla^2 \mathbb{E}_{\boldsymbol{\zeta}}[f(\mathbf{x},\boldsymbol{\zeta})] - \nabla^2 \mathbb{E}_{\boldsymbol{\zeta}}[f(\mathbf{x},\boldsymbol{\zeta})]\right\| \le \rho\|\mathbf{x}-\mathbf{y}\|, \qquad \forall \mathbf{x},\ \mathbf{y},$$

where $\|\cdot\|$ is the spectral norm for matrix and ℓ_2 norm for vector.

For a general nonconvex problem, if Assumptions 1 and 2 hold, the lower bound of the stochastic gradient complexity (a.k.a. IFO complexity) to find an ϵ-approximate first-order stationary point (ϵ-ASP) is $\Omega(\epsilon^{-4})$ [40]. Moreover, if Assumption 3 further holds, the lower complexity bound becomes $\Omega(\epsilon^{-3.5})$ for a non-variance-reduction algorithm [36].

Lipschitz Gradient. Theorem 1 with proof in Appendix Sec. B.3 proves the convergence of Adan on problem (6) with Lipschitz gradient condition.

Theorem 1. *Suppose that Assumptions 1 and 2 hold. Let $\max\{\beta_1,\beta_2\} = \mathcal{O}(\epsilon^2)$, $\mu := \sqrt{2}\beta_3 c_\infty/\varepsilon \ll 1$, $\eta = \mathcal{O}(\epsilon^2)$, and $\lambda_k = \lambda(1-\mu)^k$. Algorithm 1 runs at most $K = \Omega\big(c_\infty^{2.5}\epsilon^{-4}\big)$ iterations to achieve:*

$$\frac{1}{K+1}\sum\nolimits_{k=0}^{K}\mathbb{E}\Big(\|\nabla F_k(\boldsymbol{\theta}_k)\|^2\Big) \le 4\epsilon^2.$$

That is, to find an ϵ-ASP, the stochastic gradient complexity of Adan on problem (6) is $\mathcal{O}\big(c_\infty^{2.5}\epsilon^{-4}\big)$.

Theorem 1 shows that under Assumptions 1 and 2, Adan can converge to an ϵ-ASP of a nonconvex stochastic problem with stochastic gradient complexity $\mathcal{O}\big(c_\infty^{2.5}\epsilon^{-4}\big)$ which accords with the lower bound $\Omega(\epsilon^{-4})$ in [40]. For this convergence, Adan has no requirement on minibatch size and only assumes gradient estimation to be unbiased and bounded. Moreover, as shown in Table 1 in Sec. 1, the complexity of Adan is superior to those of previous adaptive gradient algorithms. For Adabelief and LAMB, Adan always has lower complexity and respectively enjoys $d^3\times$ and $d^2\times$ lower complexity for the worst case. Adam-type optimizers (*e.g.* Adam and AMSGrad) enjoy the same complexity as Adan. But they cannot separate the ℓ_2 regularizer with the objective like AdamW and Adan. Namely, they always solve a static loss $F(\cdot)$ rather than a dynamic loss $F_k(\cdot)$. The regularizer separation can boost generalization performance [19, 20] and already helps AdamW dominate training of ViT-alike architectures. Besides, some previous analyses [13, 14, 63, 64] need the momentum coefficient (i.e. βs) to be close or increased to one, which contradicts with the practice that βs are close to zero. In contrast, Theorem 1 assumes that all βs are very small, which is more consistent with the practice. Note that when $\mu = c/T$, we have $\lambda_k/\lambda \in [(1-c),1]$ during training. Hence we could choose the λ_k as a fixed constant in the experiment for convenience.

Lipschitz Hessian. To further improve the theoretical convergence speed, we introduce Assumption 3, and set a proper restart condition to reset the momentum during training. Consider an extension point $\mathbf{y}_{k+1} := \boldsymbol{\theta}_{k+1} + \boldsymbol{\eta}_k \circ [\mathbf{m}_k + (1-\beta_2)\mathbf{v}_k - \beta\mathbf{g}_k]$, and the restart condition is:

$$(k+1)\sum\nolimits_{t=0}^{k}\|\mathbf{y}_{t+1}-\mathbf{y}_t\|^2_{\sqrt{\mathbf{n}_t}} > R^2, \tag{7}$$

where the constant R controls the restart frequency. Intuitively, when the parameters have accumulated enough updates, the iterate may reach a new local basin. Resetting the momentum at this moment helps Adan to better use the local geometric information. Besides, we change $\boldsymbol{\eta}_k$ from $\eta/\big(\sqrt{\mathbf{n}_k}+\varepsilon\big)$ to $\eta/\big(\sqrt{\mathbf{n}_{k-1}}+\varepsilon\big)$ to ensure $\boldsymbol{\eta}_k$ to be independent of noise $\boldsymbol{\zeta}_k$. See its proof in Appendix B.4.

Theorem 2. *Suppose that Assumptions 1-3 hold. Let $R = \mathcal{O}\big(\epsilon^{0.5}\big)$, $\max\{\beta_1,\beta_2\} = \mathcal{O}\big(\epsilon^2\big)$, $\beta_3 = \mathcal{O}\big(\epsilon^4\big)$, $\eta = \mathcal{O}\big(\epsilon^{1.5}\big)$, $K = \mathcal{O}\big(\epsilon^{-2}\big)$, $\lambda = 0$. Then Algorithm 1 with restart condition Eqn. (7) satisfies:*

$$\mathbb{E}\left(\left\|\nabla F_k(\bar{\boldsymbol{\theta}})\right\|\right) = \mathcal{O}\big(c_\infty^{0.5}\epsilon\big), \quad \textit{where } \bar{\boldsymbol{\theta}} := \frac{1}{K_0}\sum_{k=1}^{K_0}\boldsymbol{\theta}_k,$$

and $K_0 = \operatorname{argmin}_{\lfloor\frac{K}{2}\rfloor\le k\le K-1}\|\mathbf{y}_{t+1}-\mathbf{y}_t\|^2_{\sqrt{\mathbf{n}_t}}$. Moreover, to find an ϵ-ASP, Algorithm 1 restarts at most $\mathcal{O}\big(c_\infty^{0.5}\epsilon^{-1.5}\big)$ times in which each restarting cycle has at most $K = \mathcal{O}\big(\epsilon^{-2}\big)$ iterations, and hence needs at most $\mathcal{O}\big(c_\infty^{1.25}\epsilon^{-3.5}\big)$ stochastic gradient complexity.

From Theorem 2, one can observe that with an extra Hessian condition, Assumption 3, Adan improves its stochastic gradient complexity from $\mathcal{O}\big(c_\infty^{2.5}\epsilon^{-4}\big)$ to $\mathcal{O}\big(c_\infty^{1.25}\epsilon^{-3.5}\big)$, which also matches

Table 2: Top-1 Acc. (%) of ResNet and ConvNext on ImageNet under the official settings. $*$ and $\diamond$ are from [4, 65].

Epoch	ResNet-50			ResNet-101		
	100	200	300	100	200	300
SAM [33]	77.3	78.7	79.4	79.5	81.1	81.6
SGD-M [26–28]	77.0	78.6	79.3	79.3	81.0	81.4
Adam [18]	76.9	78.4	78.8	78.4	80.2	80.6
AdamW [22]	77.0	78.9	79.3	78.9	79.9	80.4
LAMB [25, 65]	77.0	79.2	79.8*	79.4	81.1	81.3*
Adan (ours)	**78.1**	**79.7**	**80.2**	**79.9**	**81.6**	**81.8**

Epoch	ConvNext Tiny	
	150	300
AdamW [4, 22]	81.2	82.1$^\diamond$
Adan (ours)	**81.7**	**82.4**
Epoch	ConvNext Small	
	150	300
AdamW [4, 22]	82.2	83.1$^\diamond$
Adan (ours)	**82.5**	**83.3**

Table 3: Top-1 accuracy (%) of ResNet18 under the official setting in [2]. $*$ are reported in [15].

Adan	SGD [7]	Nadam [49]	Adam [18]	Radam [14]	Padam [38]	LAMB [25]	AdamW [22]	AdaBlief [15]	Adai [66]
70.90	70.23*	68.82	63.79*	67.62*	70.07	68.46	67.93*	70.08*	69.68

the corresponding lower bound $\Omega(\epsilon^{-3.5})$ [36]. This complexity is lower than $\mathcal{O}\big(\epsilon^{-3.5}\log\frac{c_2}{\epsilon}\big)$ of A-NIGT [34] and $\mathcal{O}\big(\epsilon^{-3.625}\big)$ of Adam$^+$ [35]. For other DNN optimizers, *e.g.* Adam, their convergence under Lipschitz Hessian condition has not been proved yet.

Moreover, Theorem 2 still holds for the large batch size. For example, by using minibatch size $b=\mathcal{O}\big(\epsilon^{-1.5}\big)$, our results still hold when $R=\mathcal{O}\big(\epsilon^{0.5}\big)$, $\max\{\beta_1,\beta_2\}=\mathcal{O}\big(\epsilon^{0.5}\big)$, $\beta_3=\mathcal{O}(\epsilon)$, $\eta=\mathcal{O}(1)$, $K=\mathcal{O}\big(\epsilon^{-0.5}\big)$, and $\lambda=0$. In this case, our η is of the order $\mathcal{O}(1)$, and is much larger than $\mathcal{O}(\mathrm{ploy}(\epsilon))$ of other optimizers (*e.g.*, LAMB [25] and Adam$^+$) for handling large minibatch. This large step size often boosts convergence speed in practice, which is actually desired.

5 Experimental Results

We evaluate Adan on vision tasks, natural language processing (NLP) tasks and reinforcement learning (RL) tasks. For vision classification tasks, we test Adan on several representative SoTA backbones under the conventional supervised settings, including 1) CNN-type architectures (ResNets [2] and ConvNexts [4]) and 2) ViTs (ViTs [3, 19] and Swins [20]). We also investigate Adan via the self-supervised pretraining by using it to train MAE-ViT [41]. Moreover, we test Adan on the vision object detection and instance segmentation tasks with two frameworks Deformable-DETR [67] and Mask-RCNN[68] (choosing ConvNext [4] as the backbone). For NLP tasks, we train LSTM [42], Transformer-XL [43], and BERT [44] for sequence modeling. We also provide the Adan's results on large language models, like GPT-2 [45], on the code generation tasks. On RL tasks, we evaluate Adan on four games in MuJoCo [69].

We compare Adan with the model's default/SoTA optimizer in all the experiments but may miss some representative optimizers, *e.g.*, Adai, Padam, and AdaBlief in some cases. This is because they report few results for larger-scale experiments. For instance, Adablief only tests ResNet-18 performance on ImageNet and actually does not test any other networks. So it is really hard for us to compare them on ViTs, Swins, ConvNext, MAEs, etc, due to the challenges for hyper-parameter tuning and limited GPU resources. The other reason is that some optimizers may fail or achieve poor performance on transformers. For example, SGD and Adam achieve much lower accuracy than AdamW. See Table 5.

5.1 Experiments for Vision Classification Tasks

5.1.1 Training Setting

Besides the vanilla supervised training setting used in ResNets [2], we further consider the following two prevalent training settings on ImageNet [70].

Training Setting I. The recently proposed "A2 training recipe" in [65] has pushed the performance limits of many SoTA CNN-type architectures by using stronger data augmentation and more training iterations. For example, on ResNet50, it sets new SoTA 80.4%, and improves the accuracy 76.1% under vanilla setting in [2]. Specifically, for data augmentation, this setting uses random crop, horizontal flipping, Mixup (0.1) [71]/CutMix (1.0) [72] with probability 0.5, and RandAugment [73]

Table 4: Top-1 ACC. (%) of ViT and Swin on ImageNet. We use their official Training Setting II to train them. $*$ and $\diamond$ are respectively reported in [19, 20]

Epoch	ViT Small		ViT Base		Swin Tiny		Swin small		Swin Base	
	150	300	150	300	150	300	150	300	150	300
AdamW [19, 20, 22]	78.3	79.9*	79.5	81.8*	79.9	81.2$^\diamond$	82.1	83.2$^\diamond$	82.6	83.5$^\diamond$
Adan (ours)	**79.6**	**80.9**	**81.7**	**82.6**	**81.3**	**81.6**	**82.9**	**83.7**	**83.3**	**83.8**

with $M = 7, N = 2$ and MSTD $= 0.5$. It sets stochastic depth (0.05) [74], and adopts cosine learning rate decay and binary cross-entropy (BCE) loss. For Adan, we use batch size 2048 for ResNet and ViT.

Training Setting II. We follow the same official training procedure of ViT/Swin/ConvNext. For this setting, data augmentation includes random crop, horizontal flipping, Mixup (0.8), CutMix (1.0), RandAugment ($M = 9$, MSTD $= 0.5$) and Random Erasing ($p = 0.25$). We use CE loss, the cosine decay for base learning rate, the stochastic depth (with official parameters), and weight decay. For Adan, we set batch size 2048 for Swin/ViT/ConvNext and 4096 for MAE. We follow MAE and tune β_3 as 0.1.

5.1.2 Results on CNN-type Architectures

To train ResNet and ConvNext, we respectively use their official Training Setting I and II. For ResNet/ConvNext, its default official optimizer is LAMB/AdamW. From Table 2, one can observe that on ResNet, 1) in most cases, Adan only running 200 epochs can achieve higher or comparable top-1 accuracy on ImageNet [70] compared with the official SoTA result trained by LAMB with 300 epochs; 2) Adan gets more improvements over other optimizers, when training is insufficient, *e.g.* 100 epochs. The possible reason for observation 1) is the regularizer separation, which can dynamically adjust the weight decay for each coordinate instead of sharing a common one like LAMB. For observation 2), this can be explained by the faster convergence speed of Adan than other optimizers. As shown in Table 1, Adan converges faster than many adaptive gradient optimizers. This faster speed partially comes from its large learning rate guaranteed by Theorem 2, almost $3\times$ larger than that of LAMB, since the same as Nestrov acceleration, Adan also looks ahead for possible correction. Note, we have tried to adjust learning rate and warmup-epoch for Adam and LAMB, but observed unstable training behaviors. On ConvNext (tiny and small), one can observe similar comparison results on ResNet.

Since some well-known deep optimizers test ResNet18 for 90 epochs under the official vanilla training setting [2], we also run Adan 90 epochs under this setting for more comparison. Table 3 shows that Adan consistently outperforms SGD and all compared adaptive optimizers. Note for this setting, it is not easy for adaptive optimizers to surpass SGD due to the absence of heavy-tailed noise, which is the crucial factor helping adaptive optimizers beat AGD [75].

5.1.3 Results on ViTs

Supervised Training. We train ViT and Swin under their official training setting, i.e. Training Setting II. Table 4 shows that across different model sizes of ViT and Swin, Adan outperforms the official AdamW optimizer by a large margin. For ViTs, their gradient per iteration differs much from the previous one due to the much sharper loss landscape than CNNs [76] and the strong random augmentations for training. So it is hard to train ViTs to converge within a few epochs. Thanks to its faster convergence, as shown in Figure 1, Adan is very suitable for this situation. Moreover, the direction correction term from the gradient difference $\mathbf{v}_k$ of Adan can also better correct the first- and second-order moments. One piece of evidence is that the first-order moment decay coefficient $\beta_1 = 0.02$ of Adan is much smaller than 0.1 used in other deep optimizers.

Besides AdamW, we also compare Adan with several other popular optimizers, including Adam, SGD-M, and LAMB, on ViT-S. Table 5 shows that SGD, Adam, and LAMB perform poorly on ViT-S, which is also observed in the works [29, 77]. These results demonstrate that the decoupled weight decay in Adan and AdamW is much more effective than 1) the vanilla weight decay, namely the commonly used ℓ_2 regularization in SGD, and 2) the one without any weight decay, since as shown in Eqn. (6), the decoupled weight decay is a dynamic regularization along the training trajectory and could better regularize the loss. Compared with AdamW, the advantages of Adan mainly come from its faster convergence shown in Figure 1 (b). We will discuss this below.

Table 5: Top-1 accuracy (%) of different optimizers when training ViT-S on ImageNet trained under training setting II. * is reported in [19].

Epoch	100	150	200	300
AdamW [19, 22] (default)	76.1	78.9	79.2	79.9*
Adam [18]	62.0	64.0	64.5	66.7
SGD-M [26–28] (AGD)	64.3	68.7	71.4	73.9
LAMB [25]	69.4	73.8	75.9	77.7
Adan (ours)	**77.5**	**79.6**	**80.0**	**80.9**

Table 6: Top-1 accuracy (%) of ViT-B and ViT-L trained by self-supervised MAE on ImageNet. We use the official Training Setting II of MAE to train ViT-B and ViT-L. $*$ and $\diamond$ are respectively reported in [78], [41].

	MAE-ViT-B			MAE-ViT-L	
Epoch	300	800	1600	800	1600
AdamW [22, 41]	82.9*	—	83.6$\diamond$	85.4$\diamond$	85.9$\diamond$
Adan	**83.4**	**83.8**	—	**85.9**	—

Self-supervised MAE Training (pre-train + finetune). We follow the MAE training framework to pre-train and finetune ViT-B on ImageNet, i.e. 300/800 pretraining epochs and 100 fine-tuning epochs. Table 6 shows that 1) with 300 pre-training epochs, Adan makes 0.5% improvement over AdamW; 2) Adan pre-trained 800 epochs surpasses AdamW pre-trained 1,600 epochs by non-trial 0.2%. All these results show the superior convergence and generalization performance of Adan.

Large-Batch Training. Although large batch size can increase computation parallelism to reduce training time and is heavily desired, optimizers often suffer performance degradation, or even fail. For instance, AdamW fails to train ViTs when batch size is beyond 4,096. How to solve the problem remains open [30]. At present, LAMB is the most effective optimizer for large batch size. Table 7 reveals that Adan is robust to batch sizes from 2k to 32k, and shows higher performance and robustness than LAMB.

Table 7: Top-1 accuracy (%) of ViT-S on ImageNet under the Training Setting I.

Batch Size	1k	2k	4k	8k	16k	32k
LAMB [25, 30]	78.9	79.2	79.8	79.7	79.5	78.4
Adan (ours)	**80.9**	**81.1**	**81.1**	**80.8**	**80.5**	**80.2**

5.1.4 Comparison of Convergence Speed

In Figure 1 (a), we plot the curve of training and test loss along with the training epochs on ResNet50. One can observe that Adan converges faster than the compared baselines and enjoys the smallest training and test losses. This demonstrates its fast convergence property and good generalization ability. To sufficiently investigate the fast convergence of Adan, we further plot the curve of training and test loss on the ViT-Small in Figure 1 (b). From the results, we can see that Adan consistently shows faster convergence behaviors than other baselines in terms of both training loss and test loss. This also partly explains the good performance of Adan.

5.2 Experiments for Language Processing Tasks

Table 8: Test perplexity (the lower, the better) on Penn Treebank for one-, two- and three-layered LSTMs. All results except Adan and Padam in the table are reported by AdaBelief [15].

LSTM	**Adan**	AdaBelief [15]	SGD [7]	AdaBound [13]	Adam [18]	AdamW [22]	Padam [38]	RAdam [14]	Yogi [63]
1 layer	**83.6**	84.2	85.0	84.3	85.9	84.7	84.2	86.5	86.5
2 layers	**65.2**	66.3	67.4	67.5	67.3	72.8	67.2	72.3	71.3
3 layers	**59.8**	61.2	63.7	63.6	64.3	69.9	63.2	70.0	67.5

5.2.1 Results on LSTM

To begin with, we test our Adan on LSTM [42] by using the Penn TreeBank dataset [79], and report the perplexity (the lower, the better) on the test set in Table 8. We follow the exact experimental setting in Adablief [15]. Indeed, all our implementations are also based on the code provided by Adablief [15][1]. We use the default setting for all the hyper-parameters provide by Adablief, since it provides more baselines for fair comparison. For Adan, we utilize its default weight decay (0.02) and βs ($\beta_1 = 0.02, \beta_2 = 0.08$, and $\beta_3 = 0.01$). We choose learning rate as 0.01 for Adan.

[1]The reported results in [15] slightly differ from the those in [38] because of their different settings for LSTM and training hyper-parameters.

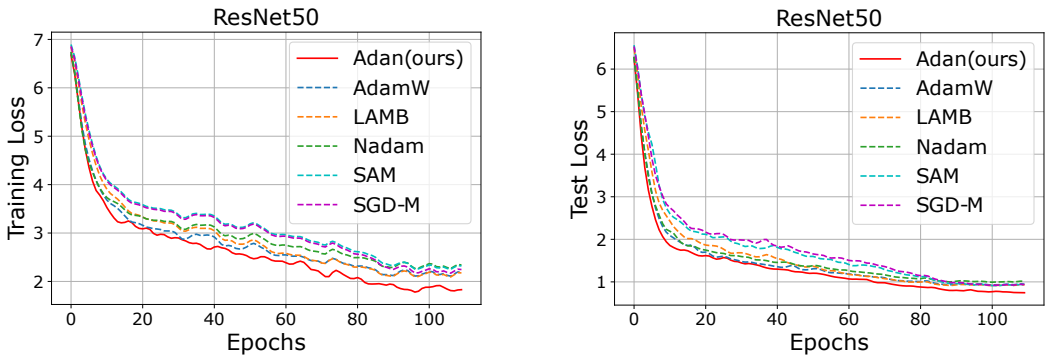

(a) Training and test curves on ResNet-50 under Training Setting I.

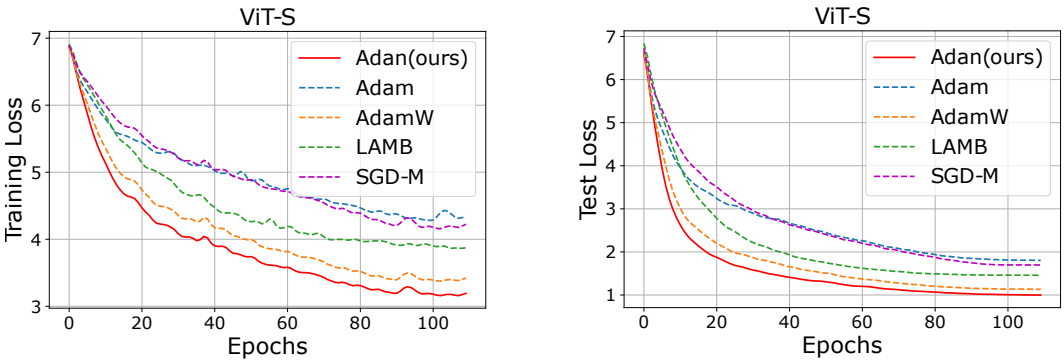

(b) Training and test curves on ViT-S under Training Setting II.

Figure 1: Training and test curves of various optimizers on ImageNet dataset. Training loss is larger due to its stronger data argumentation.

Table 9: Correlation or ACC. (%) (the higher, the better) of BERT-base model on the development set of GLUE.

BERT-base	MNLI	QNLI	QQP	RTE	SST-2	CoLA	STS-B	**Average**
Adam [18] (from [80])	83.7/84.8	89.3	90.8	71.4	91.7	48.9	91.3	81.5
Adam [18] (reproduced)	84.9/84.9	90.8	90.9	69.3	92.6	58.5	88.7	82.5
Adan (ours)	**85.7/85.6**	**91.3**	**91.2**	**73.3**	**93.2**	**64.6**	**89.3**	**84.3 (+1.8)**

Table 8 shows that on the three LSTM models, Adan always achieves the lowest perplexity, making about 1.0 overall average perplexity improvement over the runner-up. Moreover, when the LSTM depth increases, the advantage of Adan becomes more remarkable.

5.2.2 Results on BERT

Similar to the pretraining experiments of MAE which is also a self-supervised learning framework on vision tasks, we utilize Adan to train BERT [44] from scratch, which is one of the most widely used pretraining models/frameworks for NLP tasks. We employ the exact BERT training setting in the widely used codebase—Fairseq [81]. We replace the default Adam optimizer in BERT with our Adan for both pretraining and fune-tuning. Specifically, we first pretrain BERT-base on the Bookcorpus and Wikipedia datasets, and then finetune BERT-base separately for each GLUE task on the corresponding training data. Note, GLUE is a collection of 9 tasks/datasets to evaluate natural language understanding systems, in which the tasks are organized as either single-sentence classification or sentence-pair classification.

Here we simply replace the Adam optimizer in BERT with our Adan and do not make other changes, *e.g.* random seed, warmup steps and learning rate decay strategy, dropout probability, *etc*. For pretraining, we use Adan with its default weight decay (0.02) and βs ($\beta_1 = 0.02, \beta_2 = 0.08$, and $\beta_3 = 0.01$), and choose learning rate as 0.001. For fine-tuning, we consider a limited hyper-parameter sweep for each task, with a batch size of 16, and learning rates $\in \{2e-5, 4e-5\}$ and use Adan with $\beta_1 = 0.02, \beta_2 = 0.01$, and $\beta_3 = 0.01$ and weight decay 0.01.

Table 10: Pass@k metric (the higher, the better), evaluating functional correctness, for GPT-2 (345M) model on the HumanEval dataset pre-trained with different steps.

GPT-2 (345m)	Steps	pass@1	pass@10	pass@100
Adam	300k	0.0840	0.209	0.360
Adan	150k	**0.0843**	**0.221**	**0.377**

Table 11: Test PPL (the lower, the better) for Transformer-XL-base model on the WikiText-103 dataset with different training steps. * is reported in the official implementation.

Transformer-XL-base	Training Steps 50k	100k	200k
Adam [18]	28.5	25.5	24.2*
Adan (ours)	**26.2**	**24.2**	**23.5**

Following the conventional setting, we run each fine-tuning experiment three times and report the median performance in Table 9. On MNLI, we report the mismatched and matched accuracy. And we report Matthew's Correlation and Person Correlation on the task of CoLA and STS-B, respectively. The performance on the other tasks is measured by classification accuracy. The performance of our reproduced one (second row) is slightly better than the vanilla results of BERT reported in Huggingface-transformer [80] (widely used codebase for transformers in NLP), since the vanilla Bookcorpus data in [80] is not available and thus we train on the latest Bookcorpus data version.

From Table 9, one can see that in the most commonly used BERT training experiment, Adan reveals a much better advantage over Adam. Specifically, in all GLUE tasks, on the BERT-base model, Adan achieves higher performance than Adam and makes 1.8 average improvements on all tasks. In addition, on some tasks of Adan, the BERT-base trained by Adan can outperform some large models. e.g., BERT-large which achieves 70.4% on RTE, 93.2% on SST-2, and 60.6 correlation on CoLA, and XLNet-large which has 63.6 correlation on CoLA. See [82] for more results.

5.2.3 Results on GPT-2

We evaluate Adan on the large language models (LLMs), GPT-2 [45], for code generalization tasks, which enables the completion and synthesis of code, both from other code snippets and natural language descriptions. LLMs work across a wide range of domains, tasks, and programming languages, and can, for example, assist professional and citizen developers with building new applications. We pre-train GPT-2 on The-Stack dataset (Python only) [83] from BigCode[2] and evaluated on the HumanEval dataset [84] by zero-shot learning. HumanEval is used to measure functional correctness for synthesizing programs from docstrings. It consists of 164 original programming problems, assessing language comprehension, algorithms, and simple mathematics, with some comparable to simple software interview questions. We set the temperature to 0.8 during the evaluation.

We report pass@k [85] in Table 10 to evaluate the functional correctness, where k code samples are generated per problem, a problem is considered solved if any sample passes the unit tests and the total fraction of problems solved is reported. We can observe that on GPT-2, Adan surpasses its default Adam optimizer in terms of pass@k within only half pre-training steps, which implies that Adan has a much large potential in training LLMs with fewer computational costs.

5.2.4 Results on Transformer-XL

Here we investigate the performance of Adan on Transformer-XL [43] which is often used to model long sequences. We follow the exact official setting to train Transformer-XL-base on the WikiText-103 dataset that is the largest available word-level language modeling benchmark with long-term dependency. We only replace the default Adam optimizer of Transformer-XL-base by our Adan, and do not make other changes for the hyper-parameter. For Adan, we set $\beta_1 = 0.1, \beta_2 = 0.1$, and $\beta_3 = 0.001$, and choose learning rate as 0.001. We test Adan and Adam with several training steps, including 50k, 100k, and 200k (official), and report the results in Table 11.

From Table 11, one can observe that on Transformer-XL-base, Adan surpasses its default Adam optimizer in terms of test PPL (the lower, the better) under all training steps. Surprisingly, Adan using 100k training steps can even achieve comparable results to Adam with 200k training steps. All these results demonstrate the superiority of Adan over the default SoTA Adam optimizer in Transformer-XL.

[2] https://www.bigcode-project.org

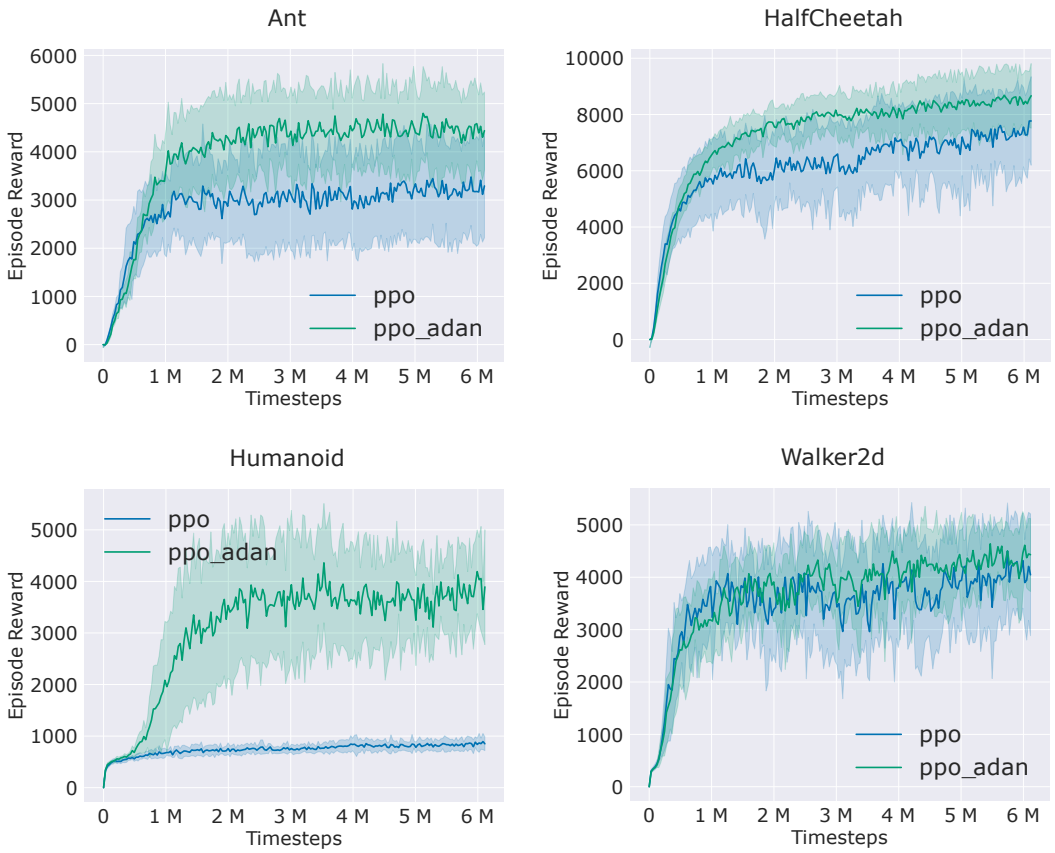

Figure 2: Comparison of PPO and our PPO-Adan on several RL games simulated by MuJoCo. Here PPO-Adan simply replaces the Adam optimizer in PPO with our Adan and does not change others.

5.3 Results on Reinforcement Learning Tasks

Here we evaluate Adan on reinforcement learning tasks. Specifically, we replace the default Adam optimizer in PPO [86] which is one of the most popular policy gradient method, and do not many any other change in PPO. For brevity, we call this new PPO version "PPO-Adan". Then we test PPO and PPO-Adan on several games which are actually continuous control environments simulated by the standard and widely-used engine, MuJoCo [69]. For these test games, their agents receive a reward at each step. Following standard evaluation, we run each game under 10 different and independent random seeds (i.e. $1 \sim 10$), and test the performance for 10 episodes every 30,000 steps. All these experiments are based on the widely used codebase Tianshou [87]. For fairness, we use the default hyper-parameters in Tianshou, *e.g.* batch size, discount, and GAE parameter. We use Adan with its default βs ($\beta_1 = 0.02, \beta_2 = 0.08$, and $\beta_3 = 0.01$). Following the default setting, we do not adopt the weight decay and choose the learning rate as 3e-4.

We report the results on four test games in Figure 2, in which the solid line denotes the averaged episodes rewards in evaluation and the shaded region is its 75% confidence intervals. From Figure 2, one can observe that on the four test games, PPO-Adan achieves much higher rewards than vanilla PPO which uses Adam as its optimizer. These results demonstrate the advantages of Adan over Adam since PPO-Adan simply replaces the Adam in PPO with our Adan and does not make other changes.

5.4 Ablation Study

5.4.1 Robustness to in momentum coefficients

Here we choose MAE to investigate the effects of the momentum coefficients (βs) to Adan, since as shown in MAE, its pre-training is actually sensitive to momentum coefficients of AdamW. To this end, following MAE, we pretrain and fine tune ViT-B on ImageNet for 800 pretraining and 100 fine-tuning

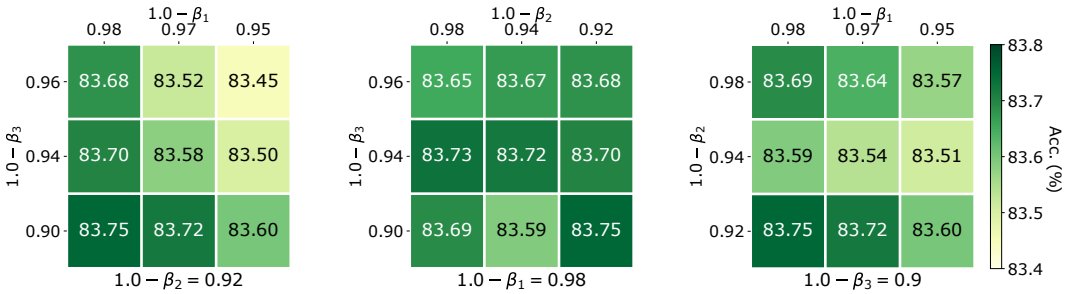

Figure 3: Effects of momentum coefficients $(\beta_1, \beta_2, \beta_3)$ to top-1 accuracy (%) of Adan on ViT-B under MAE training framework (800 pretraining and 100 fine-tuning epochs on ImageNet).

Table 12: Top-1 accuracy (%) of ViT-S on ImageNet trained under Training Setting I and II. $*$ is reported in [19].

Training epochs	Training Setting I		Training Setting II	
	AdamW [22]	Adan	AdamW [22]	Adan
150	76.4	**80.2**	78.3	**79.6**
300	77.9	**81.1**	79.9*	**80.7**

Table 13: Top-1 accuracy (%) of ViT-S and ConvNext-T on ImageNet under Training Setting II trained by 300 epochs.

	ViT Small	ConvNext Tiny
Adan w/o restart	80.71	81.38
Adan w/ restart	**80.87**	**81.62**

epochs. We also fix one of $(\beta_1, \beta_2, \beta_3)$ and tune others. Figure 3 shows that by only pretraining 800 epochs, Adan achieves $83.7\%+$ in most cases and outperforms the official accuracy 83.6% obtained by AdamW with 1600 pretraining epochs, indicating the robustness of Adan to βs. We also observe 1) Adan is not sensitive to β_2; 2) β_1 has a certain impact on Adan, namely the smaller the $(1.0 - \beta_1)$, the worse the accuracy; 3) similar to findings of MAE, a small second-order coefficient $(1.0 - \beta_3)$ can improve the accuracy. The smaller the $(1.0 - \beta_3)$, the more current landscape information the optimizer would utilize to adjust the coordinate-wise learning rate. Maybe the complex pre-training task of MAE is more preferred to the local geometric information.

5.4.2 Robustness to Training Settings

Many works [4, 19, 20, 65, 88] often preferably chose LAMB/Adam/SGD for Training Setting I and AdamW for Training Setting II. Table 12 investigates Adan under both settings and shows its consistent improvement. Moreover, one can also observe that Adan under Setting I largely improves the accuracy of Adan under Setting II. It actually surpasses the best-known accuracy 80.4% on ViT-small in [88] trained by advanced layer scale strategy and stronger data augmentation.

5.4.3 Discussion on Restart Strategy

Here we investigate the performance Adan with and without restart strategy on ViT and ConvNext under 300 training epochs. From the results in Table 13, one can observe that restart strategy slightly improves the test performance of Adan. Thus, to make our Adan simple and avoid hyper-parameter tuning of the restart strategy (e.g., restart frequency), in all experiments except Table 13, we do not use this restart strategy.

6 Conclusion

In this paper, to relieve the plague of trying different optimizers for different deep network architectures, we propose a new deep optimizer, Adan. We reformulate the vanilla AGD to a more efficient version and use it to estimate the first- and second-order moments in adaptive optimization algorithms. We prove that the complexity of Adan matches the lower bounds and is superior to those of other adaptive optimizers. Finally, extensive experimental results demonstrate that Adan consistently surpasses other optimizers on many popular backbones and frameworks, including ResNet, ConvNext, ViT, Swin, MAE-ViT, LSTM, Transformer-XL, BERT, and GPT-2.

Acknowledgment

We appreciate Qiuhao Wang from PKU, Yifei Wang from PKU, and Chengqing Wu from HUST for their valuable discussions and proof check. We are particularly grateful to Fangzhou Chen from the Chalmers University of Technology for contributing to Fusedadan.

References

[1] C. Szegedy, W. Liu, Y. Jia, P. Sermanet, S. Reed, D. Anguelov, D. Erhan, V. Vanhoucke, and A. Rabinovich. Going deeper with convolutions. In *Proceedings of the IEEE Conference on Computer Vision and Pattern Recognition*, pages 1–9, 2015.

[2] Kaiming He, Xiangyu Zhang, Shaoqing Ren, and Jian Sun. Deep residual learning for image recognition. In *Proceedings of the IEEE Conference on Computer Vision and Pattern Recognition*, pages 770–778, 2016.

[3] Alexey Dosovitskiy, Lucas Beyer, Alexander Kolesnikov, Dirk Weissenborn, Xiaohua Zhai, Thomas Unterthiner, Mostafa Dehghani, Matthias Minderer, Georg Heigold, Sylvain Gelly, et al. An image is worth 16x16 words: Transformers for image recognition at scale. In *International Conference on Learning Representations*, 2020.

[4] Zhuang Liu, Hanzi Mao, Chao-Yuan Wu, Christoph Feichtenhofer, Trevor Darrell, and Saining Xie. A convnet for the 2020s. In *Proceedings of the IEEE Conference on Computer Vision and Pattern Recognition*, pages 11976–11986, 2022.

[5] Tara N Sainath, Brian Kingsbury, Abdel-rahman Mohamed, George E Dahl, George Saon, Hagen Soltau, Tomas Beran, Aleksandr Y Aravkin, and Bhuvana Ramabhadran. Improvements to deep convolutional neural networks for LVCSR. In *2013 IEEE Workshop on Automatic Speech Recognition and Understanding*, pages 315–320. IEEE, 2013.

[6] O. Abdel-Hamid, A. Mohamed, H. Jiang, L. Deng, G. Penn, and D. Yu. Convolutional neural networks for speech recognition. *IEEE Trans. on Audio, Speech, and Language Processing*, 22(10):1533–1545, 2014.

[7] H. Robbins and S. Monro. A stochastic approximation method. *The Annals of Mathematical Statistics*, pages 400–407, 1951.

[8] D. Saad. Online algorithms and stochastic approximations. *Online Learning*, 5:6–3, 1998.

[9] John Duchi, Elad Hazan, and Yoram Singer. Adaptive subgradient methods for online learning and stochastic optimization. *Journal of Machine Learning Research*, 12(7), 2011.

[10] Tieleman Tijmen and Hinton Geoffrey. Lecture 6.5-rmsprop: Divide the gradient by a running average of its recent magnitude. *COURSERA: Neural Networks for Machine Learning*, 4, 2012.

[11] Sashank J Reddi, Satyen Kale, and Sanjiv Kumar. On the convergence of Adam and beyond. In *International Conference on Learning Representations*, 2018.

[12] Xiangyi Chen, Sijia Liu, Ruoyu Sun, and Mingyi Hong. On the convergence of a class of Adam-type algorithms for non-convex optimization. In *International Conference on Learning Representations*, 2018.

[13] Liangchen Luo, Yuanhao Xiong, Yan Liu, and Xu Sun. Adaptive gradient methods with dynamic bound of learning rate. In *International Conference on Learning Representations*, 2018.

[14] Liyuan Liu, Haoming Jiang, Pengcheng He, Weizhu Chen, Xiaodong Liu, Jianfeng Gao, and Jiawei Han. On the variance of the adaptive learning rate and beyond. In *International Conference on Learning Representations*, 2019.

[15] Juntang Zhuang, Tommy Tang, Yifan Ding, Sekhar C Tatikonda, Nicha Dvornek, Xenophon Papademetris, and James Duncan. Adabelief optimizer: Adapting stepsizes by the belief in observed gradients. *Advances in Neural Information Processing Systems*, 33:18795–18806, 2020.

[16] Byeongho Heo, Sanghyuk Chun, Seong Joon Oh, Dongyoon Han, Sangdoo Yun, Gyuwan Kim, Youngjung Uh, and Jung-Woo Ha. Adamp: Slowing down the slowdown for momentum optimizers on scale-invariant weights. In *International Conference on Learning Representations*, 2020.

[17] Pan Zhou, Xingyu Xie, and Shuicheng YAN. Win: Weight-decay-integrated nesterov acceleration for adaptive gradient algorithms. In *International Conference on Learning Representations*, 2023.

[18] Diederik P Kingma and Jimmy Ba. Adam: A method for stochastic optimization. *arXiv preprint arXiv:1412.6980*, 2014.

[19] Hugo Touvron, Matthieu Cord, Matthijs Douze, Francisco Massa, Alexandre Sablayrolles, and Hervé Jégou. Training data-efficient image transformers & distillation through attention. In *International Conference on Machine Learning*, pages 10347–10357. PMLR, 2021.

[20] Ze Liu, Yutong Lin, Yue Cao, Han Hu, Yixuan Wei, Zheng Zhang, Stephen Lin, and Baining Guo. Swin transformer: Hierarchical vision transformer using shifted windows. In *Proceedings of the IEEE International Conference on Computer Vision*, pages 10012–10022, 2021.

[21] Weihao Yu, Mi Luo, Pan Zhou, Chenyang Si, Yichen Zhou, Xinchao Wang, Jiashi Feng, and Shuicheng Yan. Metaformer is actually what you need for vision. In *Proceedings of the IEEE Conference on Computer Vision and Pattern Recognition*, pages 10819–10829, 2022.

[22] Ilya Loshchilov and Frank Hutter. Decoupled weight decay regularization. In *International Conference on Learning Representations*, 2018.

[23] Yong Liu, Siqi Mai, Xiangning Chen, Cho-Jui Hsieh, and Yang You. Towards efficient and scalable sharpness-aware minimization. In *Proceedings of the IEEE Conference on Computer Vision and Pattern Recognition*, pages 12360–12370, 2022.

[24] Yang You, Igor Gitman, and Boris Ginsburg. Large batch training of convolutional networks. *arXiv preprint arXiv:1708.03888*, 2017.

[25] Yang You, Jing Li, Sashank Reddi, Jonathan Hseu, Sanjiv Kumar, Srinadh Bhojanapalli, Xiaodan Song, James Demmel, Kurt Keutzer, and Cho-Jui Hsieh. Large batch optimization for deep learning: Training bert in 76 minutes. In *International Conference on Learning Representations*, 2019.

[26] Yurii Nesterov. A method for solving the convex programming problem with convergence rate $\mathcal{O}\big(1/k^2\big)$. In *Doklady Akademii Nauk*, volume 269, pages 543–547. Russian Academy of Sciences, 1983.

[27] Yurii Nesterov. On an approach to the construction of optimal methods of minimization of smooth convex functions. *Ekonomika i Mateaticheskie Metody*, 24(3):509–517, 1988.

[28] Yurii Nesterov. *Introductory lectures on convex optimization: A basic course*, volume 87. Springer Science & Business Media, 2003.

[29] Zachary Nado, Justin M Gilmer, Christopher J Shallue, Rohan Anil, and George E Dahl. A large batch optimizer reality check: Traditional, generic optimizers suffice across batch sizes. *arXiv preprint arXiv:2102.06356*, 2021.

[30] Xiaoxin He, Fuzhao Xue, Xiaozhe Ren, and Yang You. Large-scale deep learning optimizations: A comprehensive survey. *arXiv preprint arXiv:2111.00856*, 2021.

[31] Zhishuai Guo, Yi Xu, Wotao Yin, Rong Jin, and Tianbao Yang. A novel convergence analysis for algorithms of the Adam family. *arXiv preprint arXiv:2112.03459*, 2021.

[32] Yizhou Wang, Yue Kang, Can Qin, Huan Wang, Yi Xu, Yulun Zhang, and Yun Fu. Adapting stepsizes by momentumized gradients improves optimization and generalization. *arXiv preprint arXiv:2106.11514*, 2021.

[33] Pierre Foret, Ariel Kleiner, Hossein Mobahi, and Behnam Neyshabur. Sharpness-aware minimization for efficiently improving generalization. In *International Conference on Learning Representations*, 2021.

[34] Ashok Cutkosky and Harsh Mehta. Momentum improves normalized sgd. In *International Conference on Machine Learning*, pages 2260–2268. PMLR, 2020.

[35] Mingrui Liu, Wei Zhang, Francesco Orabona, and Tianbao Yang. Adam$^+$: A stochastic method with adaptive variance reduction. *arXiv preprint arXiv:2011.11985*, 2020.

[36] Yossi Arjevani, Yair Carmon, John C Duchi, Dylan J Foster, Ayush Sekhari, and Karthik Sridharan. Second-order information in non-convex stochastic optimization: Power and limitations. In *Conference on Learning Theory*, pages 242–299. PMLR, 2020.

[37] Dongruo Zhou, Jinghui Chen, Yuan Cao, Yiqi Tang, Ziyan Yang, and Quanquan Gu. On the convergence of adaptive gradient methods for nonconvex optimization. *arXiv preprint arXiv:1808.05671*, 2018.

[38] Jinghui Chen, Dongruo Zhou, Yiqi Tang, Ziyan Yang, Yuan Cao, and Quanquan Gu. Closing the generalization gap of adaptive gradient methods in training deep neural networks. In *Proceedings of the Twenty-Ninth International Conference on International Joint Conferences on Artificial Intelligence*, pages 3267–3275, 2021.

[39] Zhouchen Lin, Huan Li, and Cong Fang. *Accelerated optimization for machine learning*. Springer, 2020.

[40] Yossi Arjevani, Yair Carmon, John C Duchi, Dylan J Foster, Nathan Srebro, and Blake Woodworth. Lower bounds for non-convex stochastic optimization. *Mathematical Programming*, pages 1–50, 2022.

[41] Kaiming He, Xinlei Chen, Saining Xie, Yanghao Li, Piotr Dollár, and Ross Girshick. Masked autoencoders are scalable vision learners. In *Proceedings of the IEEE conference on Computer Vision and Pattern Recognition*, 2022.

[42] Jürgen Schmidhuber, Sepp Hochreiter, et al. Long short-term memory. *Neural Comput*, 9(8):1735–1780, 1997.

[43] Zihang Dai, Zhilin Yang, Yiming Yang, Jaime G Carbonell, Quoc Le, and Ruslan Salakhutdinov. Transformer-xl: Attentive language models beyond a fixed-length context. In *Proceedings of the 57th Annual Meeting of the Association for Computational Linguistics*, pages 2978–2988, 2019.

[44] Jacob Devlin Ming-Wei Chang Kenton and Lee Kristina Toutanova. BERT: Pre-training of deep bidirectional transformers for language understanding. In *Proceedings of NAACL-HLT*, pages 4171–4186, 2019.

[45] Alec Radford, Jeffrey Wu, Rewon Child, David Luan, Dario Amodei, Ilya Sutskever, et al. Language models are unsupervised multitask learners. *OpenAI blog*, 1(8):9, 2019.

[46] Boris T Polyak. Some methods of speeding up the convergence of iteration methods. *Ussr Computational Mathematics and Mathematical Physics*, 4(5):1–17, 1964.

[47] Jungmin Kwon, Jeongseop Kim, Hyunseo Park, and In Kwon Choi. Asam: Adaptive sharpness-aware minimization for scale-invariant learning of deep neural networks. In *International Conference on Machine Learning*, pages 5905–5914. PMLR, 2021.

[48] Jiawei Du, Hanshu Yan, Jiashi Feng, Joey Tianyi Zhou, Liangli Zhen, Rick Siow Mong Goh, and Vincent Tan. Efficient sharpness-aware minimization for improved training of neural networks. In *International Conference on Learning Representations*, 2022.

[49] Timothy Dozat. Incorporating nesterov momentum into Adam. In *International Conference on Learning Representations Workshops*, 2016.

[50] Moritz Hardt and Tengyu Ma. Identity matters in deep learning. In *International Conference on Learning Representations*, 2017.

[51] Bo Xie, Yingyu Liang, and Le Song. Diverse neural network learns true target functions. In *Artificial Intelligence and Statistics*, pages 1216–1224. PMLR, 2017.

[52] Yuanzhi Li and Yang Yuan. Convergence analysis of two-layer neural networks with ReLU activation. *Advances in Neural Information Processing Systems*, 30, 2017.

[53] Z. Charles and D. Papailiopoulos. Stability and generalization of learning algorithms that converge to global optima. In *International Conference on Machine Learning*, pages 745–754. PMLR, 2018.

[54] Y. Zhou and Y. Liang. Characterization of gradient dominance and regularity conditions for neural networks. In *International Conference on Learning Representations*, 2018.

[55] Pan Zhou, Hanshu Yan, Xiaotong Yuan, Jiashi Feng, and Shuicheng Yan. Towards understanding why Lookahead generalizes better than SGD and beyond. In *Advances in Neural Information Processing Systems*, 2021.

[56] Quynh Nguyen, Marco Mondelli, and Guido F Montufar. Tight bounds on the smallest eigenvalue of the neural tangent kernel for deep ReLU networks. In *International Conference on Machine Learning*, pages 8119–8129, 2021.

[57] Quynh N Nguyen and Marco Mondelli. Global convergence of deep networks with one wide layer followed by pyramidal topology. *Advances in Neural Information Processing Systems*, 33:11961–11972, 2020.

[58] Xingyu Xie, Qiuhao Wang, Zenan Ling, Xia Li, Guangcan Liu, and Zhouchen Lin. Optimization induced equilibrium networks: An explicit optimization perspective for understanding equilibrium models. *IEEE Transactions on Pattern Analysis and Machine Intelligence*, 2022.

[59] Neal Parikh and Stephen Boyd. Proximal algorithms. *Foundations and Trends in optimization*, 1(3):127–239, 2014.

[60] Zhenxun Zhuang, Mingrui Liu, Ashok Cutkosky, and Francesco Orabona. Understanding AdamW through proximal methods and scale-freeness. *Transactions on Machine Learning Research*, 2022.

[61] Huan Li and Zhouchen Lin. Restarted nonconvex accelerated gradient descent: No more polylogarithmic factor in the $\mathcal{O}\left(\epsilon^{-7/4}\right)$ complexity. In *International Conference on Machine Learning*, pages 12901–12916. PMLR, 2022.

[62] Chi Jin, Praneeth Netrapalli, and Michael I Jordan. Accelerated gradient descent escapes saddle points faster than gradient descent. In *Conference On Learning Theory*, pages 1042–1085. PMLR, 2018.

[63] Manzil Zaheer, Sashank Reddi, Devendra Sachan, Satyen Kale, and Sanjiv Kumar. Adaptive methods for nonconvex optimization. *Advances in Neural Information Processing Systems*, 31, 2018.

[64] Naichen Shi, Dawei Li, Mingyi Hong, and Ruoyu Sun. RMSProp converges with proper hyper-parameter. In *International Conference on Learning Representations*, 2020.

[65] Ross Wightman, Hugo Touvron, and Hervé Jégou. Resnet strikes back: An improved training procedure in Timm. *arXiv preprint arXiv:2110.00476*, 2021.

[66] Zeke Xie, Xinrui Wang, Huishuai Zhang, Issei Sato, and Masashi Sugiyama. Adaptive inertia: Disentangling the effects of adaptive learning rate and momentum. In *International Conference on Machine Learning*, pages 24430–24459. PMLR, 2022.

[67] Xizhou Zhu, Weijie Su, Lewei Lu, Bin Li, Xiaogang Wang, and Jifeng Dai. Deformable DETR: Deformable transformers for end-to-end object detection. In *International Conference on Learning Representations*, 2021.

[68] Kaiming He, Georgia Gkioxari, Piotr Dollár, and Ross Girshick. Mask R-CNN. In *Proceedings of the IEEE International Conference on Computer Vision*, pages 2961–2969, 2017.

[69] Emanuel Todorov, Tom Erez, and Yuval Tassa. Mujoco: A physics engine for model-based control. In *2012 IEEE/RSJ International Conference on Intelligent Robots and Systems*, pages 5026–5033. IEEE, 2012.

[70] Jia Deng, Wei Dong, Richard Socher, Li-Jia Li, Kai Li, and Li Fei-Fei. Imagenet: A large-scale hierarchical image database. In *Proceedings of the IEEE conference on Computer Vision and Pattern Recognition*, pages 248–255, 2009.

[71] Hongyi Zhang, Moustapha Cisse, Yann N Dauphin, and David Lopez-Paz. Mixup: Beyond empirical risk minimization. In *International Conference on Learning Representations*, 2018.

[72] Sangdoo Yun, Dongyoon Han, Seong Joon Oh, Sanghyuk Chun, Junsuk Choe, and Youngjoon Yoo. Cutmix: Regularization strategy to train strong classifiers with localizable features. In *Proceedings of the IEEE International Conference on Computer Vision*, pages 6023–6032, 2019.

[73] Ekin D Cubuk, Barret Zoph, Jonathon Shlens, and Quoc V Le. Randaugment: Practical automated data augmentation with a reduced search space. In *Proceedings of the IEEE Conference on Computer Vision and Pattern Recognition Workshops*, pages 702–703, 2020.

[74] Gao Huang, Yu Sun, Zhuang Liu, Daniel Sedra, and Kilian Q Weinberger. Deep networks with stochastic depth. In *European Conference on Computer Vision*, pages 646–661, 2016.

[75] Jingzhao Zhang, Sai Praneeth Karimireddy, Andreas Veit, Seungyeon Kim, Sashank Reddi, Sanjiv Kumar, and Suvrit Sra. Why are adaptive methods good for attention models? *Advances in Neural Information Processing Systems*, 33:15383–15393, 2020.

[76] Xiangning Chen, Cho-Jui Hsieh, and Boqing Gong. When vision transformers outperform resnets without pre-training or strong data augmentations. In *International Conference on Learning Representation*, 2022.

[77] Tete Xiao, Mannat Singh, Eric Mintun, Trevor Darrell, Piotr Dollár, and Ross Girshick. Early convolutions help transformers see better. *Advances in Neural Information Processing Systems*, 34:30392–30400, 2021.

[78] Xiaokang Chen, Mingyu Ding, Xiaodi Wang, Ying Xin, Shentong Mo, Yunhao Wang, Shumin Han, Ping Luo, Gang Zeng, and Jingdong Wang. Context autoencoder for self-supervised representation learning. *arXiv preprint arXiv:2202.03026*, 2022.

[79] Mary Ann Marcinkiewicz. Building a large annotated corpus of english: The penn treebank. *Using Large Corpora*, 273, 1994.

[80] Thomas Wolf, Lysandre Debut, Victor Sanh, Julien Chaumond, Clement Delangue, Anthony Moi, Pierric Cistac, Tim Rault, Rémi Louf, Morgan Funtowicz, Joe Davison, Sam Shleifer, Patrick von Platen, Clara Ma, Yacine Jernite, Julien Plu, Canwen Xu, Teven Le Scao, Sylvain Gugger, Mariama Drame, Quentin Lhoest, and Alexander M. Rush. Transformers: State-of-the-art natural language processing. In *Proceedings of the 2020 Conference on Empirical Methods in Natural Language Processing: System Demonstrations*, pages 38–45, Online, October 2020. Association for Computational Linguistics.

[81] Myle Ott, Sergey Edunov, Alexei Baevski, Angela Fan, Sam Gross, Nathan Ng, David Grangier, and Michael Auli. fairseq: A fast, extensible toolkit for sequence modeling. In *Proceedings of the 2019 Conference of the North American Chapter of the Association for Computational Linguistics (Demonstrations)*, pages 48–53, 2019.

[82] Yinhan Liu, Myle Ott, Naman Goyal, Jingfei Du, Mandar Joshi, Danqi Chen, Omer Levy, Mike Lewis, Luke Zettlemoyer, and Veselin Stoyanov. Roberta: A robustly optimized bert pretraining approach. *arXiv preprint arXiv:1907.11692*, 2019.

[83] Denis Kocetkov, Raymond Li, Loubna Ben Allal, Jia Li, Chenghao Mou, Carlos Muñoz Ferrandis, Yacine Jernite, Margaret Mitchell, Sean Hughes, Thomas Wolf, Dzmitry Bahdanau, Leandro von Werra, and Harm de Vries. The Stack: 3 tb of permissively licensed source code. *Preprint*, 2022.

[84] Mark Chen, Jerry Tworek, Heewoo Jun, Qiming Yuan, Henrique Ponde de Oliveira Pinto, Jared Kaplan, Harri Edwards, Yuri Burda, Nicholas Joseph, Greg Brockman, et al. Evaluating large language models trained on code. *arXiv preprint arXiv:2107.03374*, 2021.

[85] Sumith Kulal, Panupong Pasupat, Kartik Chandra, Mina Lee, Oded Padon, Alex Aiken, and Percy S Liang. Spoc: Search-based pseudocode to code. *Advances in Neural Information Processing Systems*, 32, 2019.

[86] Yan Duan, Xi Chen, Rein Houthooft, John Schulman, and Pieter Abbeel. Benchmarking deep reinforcement learning for continuous control. In *International conference on machine learning*, pages 1329–1338. PMLR, 2016.

[87] Jiayi Weng, Huayu Chen, Dong Yan, Kaichao You, Alexis Duburcq, Minghao Zhang, Yi Su, Hang Su, and Jun Zhu. Tianshou: A highly modularized deep reinforcement learning library. *Journal of Machine Learning Research*, 23(267):1–6, 2022.

[88] Hugo Touvron, Matthieu Cord, and Hervé Jégou. Deit III: Revenge of the ViT. In *European Conference on Computer Vision*, pages 516–533. Springer, 2022.

[89] Rie Johnson and Tong Zhang. Accelerating stochastic gradient descent using predictive variance reduction. *Advances in neural information processing systems*, 26, 2013.

[90] Simon S Du, Wei Hu, and Jason D Lee. Algorithmic regularization in learning deep homogeneous models: Layers are automatically balanced. *Advances in Neural Information Processing Systems*, 31, 2018.

Appendix

The appendix contains the technical proofs of convergence results of the paper entitled "Adan: Adaptive Nesterov Momentum Algorithm for Faster Optimizing Deep Models". It is structured as follows. Sec. A discuss why the lower bound for the convergence complexity is $\Omega(\epsilon^{-3.5})$ instead of $\Omega(\epsilon^{-3.0})$. And we also compare more about the constants in the convergence bounds of various optimizers in this section. After Sec. B.1, which summarizes the notations throughout this document, we provide the technical proofs of convergence results. Then Sec. B.2 provides the proof of the equivalence between AGD and reformulated AGD, i.e., the proof of Lemma 1. And then, given Lipschitz gradient condition, Sec. B.3 provides the convergence analysis in Theorem 1. Next, we show Adan's faster convergence speed with Lipschitz Hessian condition in Sec. B.4, by first reformulating our Algorithm 1 and introducing some auxiliary bounds. Finally, we present some auxiliary lemmas in Sec. B.5.

Implementation Details of Adan For fairness, in all experiments, we only replace the optimizer with Adan and tune the step size, warm-up epochs, and weight decay while fixing the other hyper-parameters, *e.g.* data augmentation, ϵ for adaptive optimizers, and model parameters. Moreover, to make Adan simple, in all experiments except Table 13 in Sec. 5.4.3, we do not use the restart strategy. For the large-batch training experiment, we use the sqrt rule to scale the learning rate: lr$=\sqrt{\frac{\text{batch size}}{256}}\times$ 6.25e-3, and respectively set warmup epochs $\{20, 40, 60, 100, 160, 200\}$ for batch size bs $=\{1k, 2k, 4k, 8k, 16k, 32k\}$. For other remaining experiments, we use the hyper-parameters: learning rate 1.5e-2 for ViT/Swin/ResNet/ConvNext and MAE fine-tuning, and 2.0e-3 for MAE pre-training according to the official settings. We set $\beta_1 = 0.02, \beta_2 = 0.08$ and $\beta_3 = 0.01$, and let weight decay be 0.02 unless noted otherwise. We clip the global gradient norm to 5 for ResNet and do not clip the gradient for ViT, Swin, ConvNext, and MAE. In the implementation, to keep consistent with Adam-type optimizers, we utilize the de-bias strategy for Adan.

A Discussion on Convergence Results

A.1 Discussion about Lower Bound

For the lower bound, as proven in [36], on the nonconvex problems with Lipschitz gradient and Hessian, for stochastic gradient-based methods with 1) unbiased and variance-bounded stochastic gradient and 2) stochastic gradient queried on the same point per iteration, their complexity lower bound is $\Omega(\epsilon^{-3.5})$ to find an ϵ-accurate first-order stationary point. For condition 2), it means that per iteration, the algorithm only queries the stochastic gradient at one point (e.g. SGD, Adam, Adan) instead of multiple points (variance-reduced algorithms, e.g. SVRG [89]). Otherwise, the complexity lower bound becomes $\Omega(\epsilon^{-3.0})$ [36].

For the nonconvex problems with Lipschitz gradient *but without* Lipschitz Hessian, the complexity lower bound is $\Theta(\epsilon^{-4})$ as shown in [40]. Note, the above Lipschitz gradient and Hessian assumption are defined on the training loss w.r.t. the variable/parameter instead of w.r.t. each datum/input ζ. We would like to clarify that our proofs are only based on the above Lipschitz gradient and Hessian assumptions and do not require the Lipschitz gradient and Hessian w.r.t. the datum/input ζ.

A.2 Discussion about Convergence Complexity

The constant-level difference among the complexities of compared optimizers is not incremental. Firstly, under the corresponding assumptions, most compared optimizers already achieve the optimal complexity in terms of the dependence on optimization accuracy ϵ, and their complexities only differ from their constant factors, *e.g.*c_2, c_∞ and d. For instance, with Lipschitz gradient but without Lipschitz Hessian, most optimizers have complexity $\mathcal{O}\big(\frac{x}{\epsilon^4}\big)$ which matches the lower bound $\mathcal{O}\big(\frac{1}{\epsilon^4}\big)$ in [40], where the constant factor x varies from different optimizers, *e.g.*$x = c_\infty^2 d$ in Adam-type optimizer, $x = c_2^6$ in Adabelief, $x = c_2^2 d$ in LAMB, and $x = c_\infty^{2.5}$ in Adan. So under the same conditions, one cannot improve the complexity dependence on ϵ but can improve the constant factors which, as discussed below, is still significant, especially for DNNs.

Secondly, the constant-level difference may cause very different complexity whose magnitudes vary by several orders on networks. This is because 1) the modern network is often large, e.g. 11 M

parameters in the small ReNet18, leading a very large d; 2) for network gradient, its ℓ_2-norm upper bound c_2 is often much larger than its ℓ_∞-norm upper bound c_∞ as observed and proved in some work [90], because the stochastic algorithms can probably adaptively adjust the parameter magnitude at different layers so that these parameter magnitudes are balanced.

Actually, we also empirically find $c_\infty = \mathcal{O}(8.2), c_2 = \mathcal{O}(430), d = 2.2 \times 10^7$ in the ViT-small across different optimizers, e.g., AdamW, Adam, Adan, LAMB. In the extreme case, under the widely used Lipschitz gradient assumption, the complexity bound of Adan is 7.6×10^6 smaller than the one of Adam, 3.3×10^{13} smaller than the one of AdaBlief, 2.1×10^{10} smaller than the one of LAMB, *etc*. For ResNet50, we also observe $c_\infty = \mathcal{O}(78), c_2 = \mathcal{O}(970), d = 2.5 \times 10^7$ which also means a large big improvement of Adan over other optimizers.

B Technical Proofs

B.1 Notation

We provide some notations that are frequently used throughout the paper. The scale c is in normal font. And the vector is in bold lowercase. Give two vectors $\mathbf{x}$ and $\mathbf{y}$, $\mathbf{x} \geq \mathbf{y}$ means that $(\mathbf{x} - \mathbf{y})$ is a non-negative vector. $\mathbf{x}/\mathbf{y}$ or $\frac{\mathbf{x}}{\mathbf{y}}$ represents the element-wise vector division. $\mathbf{x} \circ \mathbf{y}$ means the element-wise multiplication, and $(\mathbf{x})^2 = \mathbf{x} \circ \mathbf{x}$. $\langle \cdot, \cdot \rangle$ is the inner product. Given a non-negative vector $\mathbf{n} \geq 0$, we let $\|\mathbf{x}\|^2_{\sqrt{\mathbf{n}}} \coloneqq \langle \mathbf{x}, (\sqrt{\mathbf{n}} + \varepsilon) \circ \mathbf{x} \rangle$. Unless otherwise specified, $\|\mathbf{x}\|$ is the vector ℓ_2 norm. Note that $\mathbb{E}(\mathbf{x})$ is the expectation of random vector $\mathbf{x}$. For the functions $f(\cdot)$ and $g(\cdot)$, the notation $f(\epsilon) = \mathcal{O}(g(\epsilon))$ means that $\exists a > 0$, such that $\frac{f(\epsilon)}{g(\epsilon)} \leq a, \forall \epsilon > 0$. The notation $f(\epsilon) = \Omega(g(\epsilon))$ means that $\exists a > 0$, such that $\frac{f(\epsilon)}{g(\epsilon)} \geq a, \forall \epsilon > 0$. And $f(\epsilon) = \Theta(g(\epsilon))$ means that $\exists b \geq a > 0$, such that $a \leq \frac{f(\epsilon)}{g(\epsilon)} \leq b, \forall \epsilon > 0$.

B.2 Proof of Lemma 1: equivalence between the AGD and AGD II

In this section, we show how to get AGD II from AGD. For convenience, we omit the noise term $\boldsymbol{\zeta}_k$. Note that, let $\alpha \coloneqq 1 - \beta_1$:

$$\text{AGD:} \begin{cases} \mathbf{g}_k = \nabla f(\boldsymbol{\theta}_k - \eta\alpha\mathbf{m}_{k-1}) \\ \mathbf{m}_k = \alpha\mathbf{m}_{k-1} + \mathbf{g}_k \\ \boldsymbol{\theta}_{k+1} = \boldsymbol{\theta}_k - \eta\mathbf{m}_k \end{cases}.$$

We can get:

$$\begin{aligned} \boldsymbol{\theta}_{k+1} - \eta\alpha\mathbf{m}_k =& \boldsymbol{\theta}_k - \eta\mathbf{m}_k - \eta\alpha\mathbf{m}_k = \boldsymbol{\theta}_k - \eta(1+\alpha)(\alpha\mathbf{m}_{k-1} + \nabla f(\boldsymbol{\theta}_k - \eta\alpha\mathbf{m}_{k-1})) \\ =& \boldsymbol{\theta}_k - \eta\alpha\mathbf{m}_{k-1} - \eta\alpha^2\mathbf{m}_{k-1} - \eta(1+\alpha)(\nabla f(\boldsymbol{\theta}_k - \eta\alpha\mathbf{m}_{k-1})). \end{aligned} \tag{8}$$

Let

$$\begin{cases} \bar{\boldsymbol{\theta}}_{k+1} \coloneqq \boldsymbol{\theta}_{k+1} - \eta\alpha\mathbf{m}_k, \\ \bar{\mathbf{m}}_k \coloneqq \alpha^2\mathbf{m}_{k-1} + (1+\alpha)\nabla f(\boldsymbol{\theta}_k - \eta\alpha\mathbf{m}_{k-1}) = \alpha^2\mathbf{m}_{k-1} + (1+\alpha)\nabla f(\bar{\boldsymbol{\theta}}_k) \end{cases}$$

Then, by Eq.(8), we have:

$$\bar{\boldsymbol{\theta}}_{k+1} = \bar{\boldsymbol{\theta}}_k - \eta\bar{\mathbf{m}}_k. \tag{9}$$

On the other hand, we have $\bar{\mathbf{m}}_{k-1} = \alpha^2\mathbf{m}_{k-2} + (1+\alpha)\nabla f(\bar{\boldsymbol{\theta}}_{k-1})$ and :

$$\begin{aligned} \bar{\mathbf{m}}_k - \alpha\bar{\mathbf{m}}_{k-1} &= \alpha^2\mathbf{m}_{k-1} + (1+\alpha)\nabla f(\bar{\boldsymbol{\theta}}_k) - \alpha\bar{\mathbf{m}}_{k-1} \\ &= (1+\alpha)\nabla f(\bar{\boldsymbol{\theta}}_k) + \alpha^2\big(\alpha\mathbf{m}_{k-2} + \nabla f(\bar{\boldsymbol{\theta}}_{k-1})\big) - \alpha\bar{\mathbf{m}}_{k-1} \\ &= (1+\alpha)\nabla f(\bar{\boldsymbol{\theta}}_k) + \alpha\big(\alpha^2\mathbf{m}_{k-2} + \alpha\nabla f(\bar{\boldsymbol{\theta}}_{k-1}) - \bar{\mathbf{m}}_{k-1}\big) \\ &= (1+\alpha)\nabla f(\bar{\boldsymbol{\theta}}_k) + \alpha\big(\alpha^2\mathbf{m}_{k-2} + \alpha\nabla f(\bar{\boldsymbol{\theta}}_{k-1})\big) - \alpha\bar{\mathbf{m}}_{k-1} \\ &= (1+\alpha)\nabla f(\bar{\boldsymbol{\theta}}_k) - \alpha\nabla f(\bar{\boldsymbol{\theta}}_{k-1}) \\ &= \nabla f(\bar{\boldsymbol{\theta}}_k) + \alpha\big(\nabla f(\bar{\boldsymbol{\theta}}_k) - \nabla f(\bar{\boldsymbol{\theta}}_{k-1})\big). \end{aligned} \tag{10}$$

Finally, due to Eq.(9) and Eq.(10), we have:

$$\begin{cases} \bar{\mathbf{m}}_k = \alpha \bar{\mathbf{m}}_{k-1} + \Big(\nabla f(\bar{\boldsymbol{\theta}}_k) + \alpha \big(\nabla f(\bar{\boldsymbol{\theta}}_k) - \nabla f(\bar{\boldsymbol{\theta}}_{k-1}) \big) \Big) \\ \bar{\boldsymbol{\theta}}_{k+1} = \bar{\boldsymbol{\theta}}_k - \eta \bar{\mathbf{m}}_k \end{cases}$$

B.3 Convergence Analysis with Lipschitz Gradient

Before starting the proof, we first provide several notations. Let $F_k(\boldsymbol{\theta}) \coloneqq E_{\boldsymbol{\zeta}}[f(\boldsymbol{\theta}, \boldsymbol{\zeta})] + \frac{\lambda_k}{2} \|\boldsymbol{\theta}\|^2_{\sqrt{\mathbf{n}_k}}$ and $\mu \coloneqq \sqrt{2} \beta_3 c_\infty / \varepsilon$,

$$\|\mathbf{x}\|^2_{\sqrt{\mathbf{n}_k}} \coloneqq \langle \mathbf{x}, (\sqrt{\mathbf{n}_k} + \varepsilon) \circ \mathbf{x} \rangle, \quad \lambda_k = \lambda (1-\mu)^k, \quad \tilde{\boldsymbol{\theta}}_k \coloneqq (\sqrt{\mathbf{n}_k} + \varepsilon) \circ \boldsymbol{\theta}_k.$$

Lemma 2. *Assume $f(\cdot)$ is L-smooth. For*

$$\boldsymbol{\theta}_{k+1} = \operatorname*{argmin}_{\boldsymbol{\theta}} \left(\frac{\lambda_k}{2} \|\boldsymbol{\theta}\|^2_{\sqrt{\mathbf{n}_k}} + f(\boldsymbol{\theta}_k) + \langle \mathbf{u}_k, \boldsymbol{\theta} - \boldsymbol{\theta}_k \rangle + \frac{1}{2\eta} \|(\boldsymbol{\theta} - \boldsymbol{\theta}_k)\|^2_{\sqrt{\mathbf{n}_k}} \right).$$

With $\eta \le \min\{\frac{\varepsilon}{3L}, \frac{1}{10\lambda}\}$, define $\mathbf{g}_k \coloneqq \nabla f(\boldsymbol{\theta}_k)$, then we have:

$$F_{k+1}(\boldsymbol{\theta}_{k+1}) \le F_k(\boldsymbol{\theta}_k) - \frac{\eta}{4c_\infty} \left\| \mathbf{u}_k + \lambda_k \tilde{\boldsymbol{\theta}}_k \right\|^2 + \frac{\eta}{2\varepsilon} \|\mathbf{g}_k - \mathbf{u}_k\|^2.$$

Proof. We denote $\mathbf{p}_k \coloneqq \mathbf{u}_k / \big(\sqrt{\mathbf{n}_k} + \varepsilon\big)$. By the optimality condition of $\boldsymbol{\theta}_{k+1}$, we have

$$\lambda_k \boldsymbol{\theta}_k + \mathbf{p}_k = \frac{\lambda_k \tilde{\boldsymbol{\theta}}_k + \mathbf{u}_k}{\sqrt{\mathbf{n}_k} + \varepsilon} = \frac{1 + \eta \lambda_k}{\eta} (\boldsymbol{\theta}_k - \boldsymbol{\theta}_{k+1}). \tag{11}$$

Then for $\eta \le \frac{\varepsilon}{3L}$, we have:

$$\begin{aligned}
&F_{k+1}(\boldsymbol{\theta}_{k+1}) \le f(\boldsymbol{\theta}_k) + \langle \nabla f(\boldsymbol{\theta}_k), \boldsymbol{\theta}_{k+1} - \boldsymbol{\theta}_k \rangle + \frac{L}{2} \|\boldsymbol{\theta}_{k+1} - \boldsymbol{\theta}_k\|^2 + \frac{\lambda_{k+1}}{2} \|\boldsymbol{\theta}_{k+1}\|^2_{\sqrt{\mathbf{n}_{k+1}}} \\
\overset{(a)}{\le}& f(\boldsymbol{\theta}_k) + \langle \nabla f(\boldsymbol{\theta}_k), \boldsymbol{\theta}_{k+1} - \boldsymbol{\theta}_k \rangle + \frac{L}{2} \|\boldsymbol{\theta}_{k+1} - \boldsymbol{\theta}_k\|^2 + \frac{\lambda_k}{2} \|\boldsymbol{\theta}_{k+1}\|^2_{\sqrt{\mathbf{n}_k}} \\
\overset{(b)}{\le}& F_k(\boldsymbol{\theta}_k) + \left\langle \boldsymbol{\theta}_{k+1} - \boldsymbol{\theta}_k, \lambda_k \boldsymbol{\theta}_k + \frac{\mathbf{g}_k}{\sqrt{\mathbf{n}_k} + \varepsilon} \right\rangle_{\sqrt{\mathbf{n}_k}} + \frac{L/\varepsilon + \lambda_k}{2} \|\boldsymbol{\theta}_{k+1} - \boldsymbol{\theta}_k\|^2_{\sqrt{\mathbf{n}_k}} \\
=& F_k(\boldsymbol{\theta}_k) + \frac{L/\varepsilon + \lambda_k}{2} \|\boldsymbol{\theta}_{k+1} - \boldsymbol{\theta}_k\|^2_{\sqrt{\mathbf{n}_k}} + \left\langle \boldsymbol{\theta}_{k+1} - \boldsymbol{\theta}_k, \lambda_k \boldsymbol{\theta}_k + \mathbf{p}_k + \frac{\mathbf{g}_k - \mathbf{u}_k}{\sqrt{\mathbf{n}_k} + \varepsilon} \right\rangle_{\sqrt{\mathbf{n}_k}} \\
\overset{(c)}{=}& F_k(\boldsymbol{\theta}_k) + \left(\frac{L/\varepsilon + \lambda_k}{2} - \frac{1 + \eta \lambda_k}{\eta} \right) \|\boldsymbol{\theta}_{k+1} - \boldsymbol{\theta}_k\|^2_{\sqrt{\mathbf{n}_k}} + \left\langle \boldsymbol{\theta}_{k+1} - \boldsymbol{\theta}_k, \frac{\mathbf{g}_k - \mathbf{u}_k}{\sqrt{\mathbf{n}_k} + \varepsilon} \right\rangle_{\sqrt{\mathbf{n}_k}} \\
\overset{(d)}{\le}& F_k(\boldsymbol{\theta}_k) + \left(\frac{L/\varepsilon}{2} - \frac{1}{\eta} \right) \|\boldsymbol{\theta}_{k+1} - \boldsymbol{\theta}_k\|^2_{\sqrt{\mathbf{n}_k}} + \frac{1}{2\eta} \|\boldsymbol{\theta}_{k+1} - \boldsymbol{\theta}_k\|^2_{\sqrt{\mathbf{n}_k}} + \frac{\eta}{2\varepsilon} \|\mathbf{g}_k - \mathbf{u}_k\|^2 \\
\le& F_k(\boldsymbol{\theta}_k) - \frac{1}{3\eta} \|\boldsymbol{\theta}_{k+1} - \boldsymbol{\theta}_k\|^2_{\sqrt{\mathbf{n}_k}} + \frac{\eta}{2\varepsilon} \|\mathbf{g}_k - \mathbf{u}_k\|^2 \\
\le& F_k(\boldsymbol{\theta}_k) - \frac{\eta}{4c_\infty} \left\| \mathbf{u}_k + \lambda_k \tilde{\boldsymbol{\theta}}_k \right\|^2 + \frac{\eta}{2\varepsilon} \|\mathbf{g}_k - \mathbf{u}_k\|^2,
\end{aligned}$$

where (a) comes from the fact $\lambda_{k+1}(1-\mu)^{-1} = \lambda_k$ and Proposition 3: $\left(\frac{\sqrt{\mathbf{n}_k} + \varepsilon}{\sqrt{\mathbf{n}_{k+1}} + \varepsilon} \right)_i \ge 1 - \mu$, which implies:

$$\lambda_{k+1} \|\boldsymbol{\theta}_{k+1}\|^2_{\sqrt{\mathbf{n}_{k+1}}} \le \frac{\lambda_{k+1}}{1-\mu} \|\boldsymbol{\theta}_{k+1}\|^2_{\sqrt{\mathbf{n}_k}} = \lambda_k \|\boldsymbol{\theta}_{k+1}\|^2_{\sqrt{\mathbf{n}_k}},$$

and (b) is from:

$$\|\boldsymbol{\theta}_{k+1}\|^2_{\sqrt{\mathbf{n}_k}} = \left(\|\boldsymbol{\theta}_k\|^2_{\sqrt{\mathbf{n}_k}} + 2 \langle \boldsymbol{\theta}_{k+1} - \boldsymbol{\theta}_k, \boldsymbol{\theta}_k \rangle_{\sqrt{\mathbf{n}_k}} + \|\boldsymbol{\theta}_{k+1} - \boldsymbol{\theta}_k\|^2_{\sqrt{\mathbf{n}_k}} \right),$$

(c) is due to Eqn. (11), and for (d), we utilize:

$$\left\langle \boldsymbol{\theta}_{k+1}-\boldsymbol{\theta}_k, \frac{\mathbf{g}_k-\mathbf{u}_k}{\sqrt{\mathbf{n}_k}+\varepsilon}\right\rangle_{\sqrt{\mathbf{n}_k}} \leq \frac{1}{2\eta}\|\boldsymbol{\theta}_{k+1}-\boldsymbol{\theta}_k\|^2_{\sqrt{\mathbf{n}_k}}+\frac{\eta}{2\varepsilon}\|\mathbf{g}_k-\mathbf{u}_k\|^2,$$

the last inequality comes from the fact in Eqn. (11) and $\eta \leq \frac{1}{10\lambda}$, such that:

$$\frac{1}{3\eta}\|(\boldsymbol{\theta}_{k+1}-\boldsymbol{\theta}_k)\|^2_{\sqrt{\mathbf{n}_k}} = \frac{\eta}{3\big(\sqrt{\mathbf{n}_k}+\varepsilon\big)(1+\eta\lambda_k)}\left\|\mathbf{u}_k+\lambda_k\tilde{\boldsymbol{\theta}}_k\right\|^2 \geq \frac{\eta}{4c_\infty}\left\|\mathbf{u}_k+\lambda_k\tilde{\boldsymbol{\theta}}_k\right\|^2.$$

□

Theorem 1. *Suppose Assumptions 1 and 2 hold. Let* $c_l \coloneqq \frac{1}{c_\infty}$ *and* $c_u \coloneqq \frac{1}{\varepsilon}$. *With* $\beta_3 c_\infty/\varepsilon \ll 1$,

$$\eta^2 \leq \frac{c_l\beta_1^2}{8c_u^3L^2}, \quad \max\{\beta_1,\beta_2\} \leq \frac{c_l\epsilon^2}{96c_u\sigma^2}, \quad T \geq \max\left\{\frac{24\Delta_0}{\eta c_l\epsilon^2}, \frac{24c_u\sigma^2}{\beta_1 c_l\epsilon^2}\right\},$$

where $\Delta_0 \coloneqq F(\boldsymbol{\theta}_0)-f^*$ *and* $f^* \coloneqq \min_{\boldsymbol{\theta}} \mathbb{E}_{\boldsymbol{\zeta}}[\nabla f(\boldsymbol{\theta}_k,\boldsymbol{\zeta})]$, *then we let* $\mathbf{u}_k \coloneqq \mathbf{m}_k+(1-\beta_1)\mathbf{v}_k$ *and have:*

$$\frac{1}{T+1}\sum_{k=0}^{T}\mathbb{E}\left(\left\|\mathbf{u}_k+\lambda_k\tilde{\boldsymbol{\theta}}_k\right\|^2\right) \leq \epsilon^2,$$

and

$$\frac{1}{T+1}\sum_{k=0}^{T}\mathbb{E}\left(\left\|\mathbf{m}_k-\mathbf{g}_k^{full}\right\|^2\right) \leq \frac{\epsilon^2}{4}, \quad \frac{1}{T+1}\sum_{k=0}^{T}\mathbb{E}\left(\|\mathbf{v}_k\|^2\right) \leq \frac{\epsilon^2}{4}.$$

Hence, we have:

$$\frac{1}{T+1}\sum_{k=0}^{T}\mathbb{E}\left(\left\|\nabla_{\boldsymbol{\theta}_k}\left(\frac{\lambda_k}{2}\|\boldsymbol{\theta}\|^2_{\sqrt{\mathbf{n}_k}}+\mathbb{E}_{\boldsymbol{\zeta}}[\nabla f(\boldsymbol{\theta}_k,\boldsymbol{\zeta})]\right)\right\|^2\right) \leq 4\epsilon^2.$$

Proof. For convince, we let $\mathbf{u}_k \coloneqq \mathbf{m}_k+(1-\beta_1)\mathbf{v}_k$ and $\mathbf{g}_k^{full} \coloneqq \mathbb{E}_{\boldsymbol{\zeta}}[\nabla f(\boldsymbol{\theta}_k,\boldsymbol{\zeta})]$. We have:

$$\left\|\mathbf{u}_k-\mathbf{g}_k^{full}\right\|^2 \leq 2\left\|\mathbf{m}_k-\mathbf{g}_k^{full}\right\|^2+2(1-\beta_1)^2\|\mathbf{v}_k\|^2.$$

By Lemma 2, Lemma 5, and Lemma 6, we already have:

$$F_{k+1}(\boldsymbol{\theta}_{k+1}) \leq F_k(\boldsymbol{\theta}_k)-\frac{\eta c_l}{4}\left\|\mathbf{u}_k+\lambda_k\tilde{\boldsymbol{\theta}}_k\right\|^2+\eta c_u\left\|\mathbf{g}_k^{full}-\mathbf{m}_k\right\|^2+\eta c_u(1-\beta_1)^2\|\mathbf{v}_k\|^2, \quad (12)$$

$$\mathbb{E}\left(\left\|\mathbf{m}_{k+1}-\mathbf{g}_{k+1}^{full}\right\|^2\right) \leq (1-\beta_1)\mathbb{E}\left(\left\|\mathbf{m}_k-\mathbf{g}_k^{full}\right\|^2\right)+\frac{(1-\beta_1)^2L^2}{\beta_1}\mathbb{E}\left(\|\boldsymbol{\theta}_{k+1}-\boldsymbol{\theta}_k\|^2\right)+\beta_1^2\sigma^2 \quad (13)$$

$$\mathbb{E}\left(\|\mathbf{v}_{k+1}\|^2\right) \leq (1-\beta_2)\mathbb{E}\left(\|\mathbf{v}_k\|^2\right)+2\beta_2\mathbb{E}\left(\left\|\mathbf{g}_{k+1}^{full}-\mathbf{g}_k^{full}\right\|^2\right)+3\beta_2^2\sigma^2 \quad (14)$$

Then by adding Eq.(12) with $\frac{\eta c_u}{\beta_1}\times$ Eq.(13) and $\frac{\eta c_u(1-\beta_1)^2}{\beta_2}\times$ Eq.(14), we can get:

$$\begin{aligned}
\mathbb{E}(\Phi_{k+1}) \leq{}& \mathbb{E}\left(\Phi_k-\frac{\eta c_l}{4}\left\|\mathbf{u}_k+\lambda_k\tilde{\boldsymbol{\theta}}_k\right\|^2+\frac{\eta c_u}{\beta_1}\left(\frac{(1-\beta_1)^2L^2}{\beta_1}\|\boldsymbol{\theta}_{k+1}-\boldsymbol{\theta}_k\|^2+\beta_1^2\sigma^2\right)\right)\\
&+\frac{\eta c_u(1-\beta_1)^2}{\beta_2}\mathbb{E}\left(2\beta_2L^2\|\boldsymbol{\theta}_{k+1}-\boldsymbol{\theta}_k\|^2+3\beta_2^2\sigma^2\right)\\
\leq{}&\mathbb{E}\left(\Phi_k-\frac{\eta c_l}{4}\left\|\mathbf{u}_k+\lambda_k\tilde{\boldsymbol{\theta}}_k\right\|^2+\eta c_uL^2\left(\frac{(1-\beta_1)^2}{\beta_1^2}+2(1-\beta_1)^2\right)\|\boldsymbol{\theta}_{k+1}-\boldsymbol{\theta}_k\|^2\right)\\
&+(\beta_1+3\beta_2)\eta c_u\sigma^2\\
\overset{(a)}{\leq}{}&\mathbb{E}\left(\Phi_k-\frac{\eta c_l}{4}\left\|\mathbf{u}_k+\lambda_k\tilde{\boldsymbol{\theta}}_k\right\|^2+\frac{\eta c_uL^2}{\beta_1^2}\|\boldsymbol{\theta}_{k+1}-\boldsymbol{\theta}_k\|^2\right)+4\beta_m\eta c_u\sigma^2\\
\overset{(b)}{\leq}{}&\mathbb{E}\left(\Phi_k+\left(\frac{(\eta c_u)^3L^2}{\beta_1^2}-\frac{\eta c_l}{4}\right)\left\|\mathbf{u}_k+\lambda_k\tilde{\boldsymbol{\theta}}_k\right\|^2\right)+4\beta_m\eta c_u\sigma^2\\
\leq{}&\mathbb{E}\left(\Phi_k-\frac{\eta c_l}{8}\left\|\mathbf{u}_k+\lambda_k\tilde{\boldsymbol{\theta}}_k\right\|^2\right)+4\beta_m\eta c_u\sigma^2,
\end{aligned}$$

where we let:

$$\Phi_k \coloneqq F_k(\boldsymbol{\theta}_k) - f^* + \frac{\eta c_u}{\beta_1}\left\|\mathbf{m}_k - \mathbf{g}_k^{full}\right\|^2 + \frac{\eta c_u(1-\beta_1)^2}{\beta_2}\|\mathbf{v}_k\|^2,$$
$$\beta_m = \max\{\beta_1, \beta_2\} \leq \frac{2}{3}, \quad \eta \leq \frac{c_l \beta_1^2}{8 c_u^3 L^2},$$

and for (a), when $\beta_1 \leq \frac{2}{3}$, we have:

$$\frac{(1-\beta_1)^2}{\beta_1^2} + 2(1-\beta_1)^2 < \frac{1}{\beta_1^2},$$

and (b) is due to Eq.(11) from Lemma 2. And hence, we have:

$$\sum_{k=0}^{T}\mathbb{E}(\Phi_{k+1}) \leq \sum_{k=0}^{T}\mathbb{E}(\Phi_k) - \frac{\eta c_l}{8}\sum_{k=0}^{T}\left\|\mathbf{u}_k + \lambda_k\tilde{\boldsymbol{\theta}}_k\right\|^2 + (T+1)4\eta c_u \beta_m \sigma^2.$$

Hence, we can get:

$$\frac{1}{T+1}\sum_{k=0}^{T}\mathbb{E}\left(\left\|\mathbf{u}_k + \lambda_k\tilde{\boldsymbol{\theta}}_k\right\|^2\right) \leq \frac{8\Phi_0}{\eta c_l T} + \frac{32 c_u \beta \sigma^2}{c_l} = \frac{8\Delta_0}{\eta c_l T} + \frac{8 c_u \sigma^2}{\beta_1 c_l T} + \frac{32 c_u \beta_m \sigma^2}{c_l} \leq \epsilon^2,$$

where

$$\Delta_0 \coloneqq F(\boldsymbol{\theta}_0) - f^*, \quad \beta_m \leq \frac{c_l \epsilon^2}{96 c_u \sigma^2}, \quad T \geq \max\left\{\frac{24\Delta_0}{\eta c_l \epsilon^2}, \frac{24 c_u \sigma^2}{\beta_1 c_l \epsilon^2}\right\}.$$

We finish the first part of the theorem. From Eq.(13), we can conclude that:

$$\frac{1}{T+1}\sum_{k=0}^{T}\mathbb{E}\left(\left\|\mathbf{m}_k - \mathbf{g}_k^{full}\right\|^2\right) \leq \frac{\sigma^2}{\beta T} + \frac{L^2\eta^2 c_u^2 \epsilon^2}{\beta_1^2} + \beta_1\sigma^2 < \frac{\epsilon^2}{4}.$$

From Eq.(14), we can conclude that:

$$\frac{1}{T+1}\sum_{k=0}^{T}\mathbb{E}\left(\|\mathbf{v}_k\|^2\right) \leq 2L^2\eta^2 c_u^2\epsilon^2 + 3\beta_2\sigma^2 < \frac{\epsilon^2}{4}.$$

Finally we have:

$$\frac{1}{T+1}\sum_{k=0}^{T}\mathbb{E}\left(\left\|\nabla_{\boldsymbol{\theta}_k}\left(\frac{\lambda_k}{2}\|\boldsymbol{\theta}\|^2_{\sqrt{\mathbf{n}_k}} + \mathbb{E}_{\boldsymbol{\zeta}}[f(\boldsymbol{\theta}_k, \boldsymbol{\zeta})]\right)\right\|^2\right)$$
$$\leq \frac{1}{T+1}\left(\sum_{k=0}^{T}\mathbb{E}\left(2\left\|\mathbf{u}_k + \lambda_k\tilde{\boldsymbol{\theta}}_k\right\|^2 + 4\left\|\mathbf{m}_k - \mathbf{g}_k^{full}\right\|^2 + 4\|\mathbf{v}_k\|^2\right)\right) \leq 4\epsilon^2.$$

Now, we have finished the proof. □

B.4 Faster Convergence with Lipschitz Hessian

For convince, we let $\lambda = 0$, $\beta_1 = \beta_2 = \beta$ and $\beta_3 = \beta^2$ in the following proof. To consider the weight decay term in the proof, we refer to the previous section for more details. For the ease of notation, we denote $\mathbf{x}$ instead of $\boldsymbol{\theta}$ the variable needed to be optimized in the proof, and abbreviate $E_{\boldsymbol{\zeta}}[f(\boldsymbol{\theta}_k, \boldsymbol{\zeta})]$ as $f(\boldsymbol{\theta}_k)$.

B.4.1 Reformulation

We first prove the equivalent form between Algorithm 1 and Algorithm 2. The main iteration in Algorithm 1 is:

$$\begin{cases}\mathbf{m}_k = (1-\beta)\mathbf{m}_{k-1} + \beta\mathbf{g}_k, \\ \mathbf{v}_k = (1-\beta)\mathbf{v}_{k-1} + \beta((\mathbf{g}_k - \mathbf{g}_{k-1})), \\ \mathbf{x}_{k+1} = \mathbf{x}_k - \boldsymbol{\eta}_k \circ (\mathbf{m}_k + (1-\beta)\mathbf{v}_k).\end{cases}$$

Algorithm 2: Nesterov Adaptive Momentum Estimation Reformulation

Input: initial point $\boldsymbol{\theta}_0$, stepsize η, average coefficients β, and ε.

begin

  while $k < K$ **do**

    get stochastic gradient estimator $\mathbf{g}_k$ at $\mathbf{x}_k$;

    $\hat{\mathbf{m}}_k = (1-\beta)\hat{\mathbf{m}}_{k-1} + \beta(\mathbf{g}_k + (1-\beta)(\mathbf{g}_k - \mathbf{g}_{k-1}))$;

    $\mathbf{n}_k = \big(1-\beta^2\big)\mathbf{n}_{k-1} + \beta^2(\mathbf{g}_{k-1} + (1-\beta)(\mathbf{g}_{k-1} - \mathbf{g}_{k-2}))^2$;

    $\boldsymbol{\eta}_k = \eta/\big(\sqrt{\mathbf{n}_k} + \varepsilon\big)$;

    $\mathbf{y}_{k+1} = \mathbf{x}_k - \boldsymbol{\eta}_k\beta\mathbf{g}_k$;

    $\mathbf{x}_{k+1} = \mathbf{y}_{k+1} + (1-\beta)[(\mathbf{y}_{k+1} - \mathbf{y}_k) + (\boldsymbol{\eta}_{k-1} - \boldsymbol{\eta}_k)(\hat{\mathbf{m}}_{k-1} - \beta\mathbf{g}_{k-1})]$;

    if $(k+1)\sum_{t=0}^{k}\left\|\big(\sqrt{\mathbf{n}_t} + \varepsilon\big)^{1/2} \circ (\mathbf{y}_{t+1} - \mathbf{y}_t)\right\|^2 \geq R^2$ **then**

      get stochastic gradient estimator $\mathbf{g}_0$ at $\mathbf{x}_{k+1}$;

      $\hat{\mathbf{m}}_0 = \mathbf{g}_0, \quad \mathbf{n}_0 = \mathbf{g}_0^2, \quad \mathbf{x}_0 = \mathbf{y}_0 = \mathbf{x}_{k+1}, \quad \mathbf{x}_1 = \mathbf{y}_1 = \mathbf{x}_0 - \eta\frac{\hat{\mathbf{m}}_0}{\sqrt{\mathbf{n}_0}+\varepsilon}, \quad k = 1;$

    end if

  end while

  $K_0 = \operatorname{argmin}_{\lfloor \frac{K}{2} \rfloor \leq k \leq K-1}\left\|\big(\sqrt{\mathbf{n}_k} + \varepsilon\big)^{1/2} \circ (\mathbf{y}_{k+1} - \mathbf{y}_k)\right\|$;

end

Output: $\bar{\mathbf{x}} \coloneqq \frac{1}{K_0}\sum_{k=1}^{K_0}\mathbf{x}_k$

Let $\hat{\mathbf{m}}_k \coloneqq (\mathbf{m}_k + (1-\beta)\mathbf{v}_k)$, we can simplify the variable:

$$\begin{cases}\hat{\mathbf{m}}_k = (1-\beta)\hat{\mathbf{m}}_{k-1} + \beta(\mathbf{g}_k + (1-\beta)(\mathbf{g}_k - \mathbf{g}_{k-1})),\\ \mathbf{x}_{k+1} = \mathbf{x}_k - \boldsymbol{\eta}_k \circ \hat{\mathbf{m}}_k.\end{cases}$$

We let $\mathbf{y}_{k+1} \coloneqq \mathbf{x}_{k+1} + \boldsymbol{\eta}_k(\hat{\mathbf{m}}_k - \beta\mathbf{g}_k)$, then we can get:

$$\mathbf{y}_{k+1} = \mathbf{x}_{k+1} + \boldsymbol{\eta}_k\hat{\mathbf{m}}_k - \beta\boldsymbol{\eta}_k\mathbf{g}_k = \mathbf{x}_{k+1} + \mathbf{x}_k - \mathbf{x}_{k+1} - \beta\boldsymbol{\eta}_k\mathbf{g}_k = \mathbf{x}_k - \beta\boldsymbol{\eta}_k\mathbf{g}_k.$$

On one hand, we have: $\mathbf{x}_{k+1} = \mathbf{x}_k - \boldsymbol{\eta}_k\hat{\mathbf{m}}_k = \mathbf{y}_{k+1} - \boldsymbol{\eta}_k(\hat{\mathbf{m}}_k - \beta\mathbf{g}_k)$. On the other hand:

$$\begin{aligned}\boldsymbol{\eta}_k(\hat{\mathbf{m}}_k - \beta\mathbf{g}_k) =& (1-\beta)\boldsymbol{\eta}_k(\hat{\mathbf{m}}_{k-1} + \beta(\mathbf{g}_k - \mathbf{g}_{k-1}))\\ =& (1-\beta)\boldsymbol{\eta}_k(\hat{\mathbf{m}}_{k-1} + \beta(\mathbf{g}_k - \mathbf{g}_{k-1}))\\ =& (1-\beta)\boldsymbol{\eta}_k\left(\frac{\mathbf{x}_{k-1} - \mathbf{x}_k}{\boldsymbol{\eta}_{k-1}} + \beta(\mathbf{g}_k - \mathbf{g}_{k-1})\right)\\ =& (1-\beta)\frac{\boldsymbol{\eta}_k}{\boldsymbol{\eta}_{k-1}}(\mathbf{x}_{k-1} - \mathbf{x}_k + \beta\boldsymbol{\eta}_{k-1}(\mathbf{g}_k - \mathbf{g}_{k-1}))\\ =& (1-\beta)\frac{\boldsymbol{\eta}_k}{\boldsymbol{\eta}_{k-1}}(\mathbf{y}_k - \mathbf{x}_k + \beta\boldsymbol{\eta}_{k-1}\mathbf{g}_k)\\ =& (1-\beta)\left[\frac{\boldsymbol{\eta}_k}{\boldsymbol{\eta}_{k-1}}(\mathbf{y}_k - \mathbf{y}_{k+1} - \beta(\boldsymbol{\eta}_k - \boldsymbol{\eta}_{k-1})\mathbf{g}_k)\right]\\ =& (1-\beta)\left[(\mathbf{y}_k - \mathbf{y}_{k+1}) + \frac{\boldsymbol{\eta}_k - \boldsymbol{\eta}_{k-1}}{\boldsymbol{\eta}_{k-1}}(\mathbf{y}_k - \mathbf{y}_{k+1} - \beta\boldsymbol{\eta}_k\mathbf{g}_k)\right]\\ =& (1-\beta)\left[(\mathbf{y}_k - \mathbf{y}_{k+1}) + \frac{\boldsymbol{\eta}_k - \boldsymbol{\eta}_{k-1}}{\boldsymbol{\eta}_{k-1}}(\mathbf{y}_k - \mathbf{x}_k)\right]\\ =& (1-\beta)[(\mathbf{y}_k - \mathbf{y}_{k+1}) + (\boldsymbol{\eta}_k - \boldsymbol{\eta}_{k-1})(\mathbf{m}_{k-1} - \beta\mathbf{g}_{k-1})].\end{aligned}$$

Hence, we can conclude that:

$$\mathbf{x}_{k+1} = \mathbf{y}_{k+1} + (1-\beta)[(\mathbf{y}_{k+1} - \mathbf{y}_k) + (\boldsymbol{\eta}_{k-1} - \boldsymbol{\eta}_k)(\hat{\mathbf{m}}_{k-1} - \beta\mathbf{g}_{k-1})].$$

The main iteration in Algorithm 1 becomes:

$$\begin{cases}\mathbf{y}_{k+1} = \mathbf{x}_k - \beta\boldsymbol{\eta}_k\mathbf{g}_k,\\ \mathbf{x}_{k+1} = \mathbf{y}_{k+1} + (1-\beta)\left[(\mathbf{y}_{k+1} - \mathbf{y}_k) + \frac{\boldsymbol{\eta}_{k-1} - \boldsymbol{\eta}_k}{\boldsymbol{\eta}_{k-1}}(\mathbf{y}_k - \mathbf{x}_k)\right].\end{cases} \tag{15}$$

B.4.2 Auxiliary Bounds

We first show some interesting property. Define $\mathcal{K}$ to be the iteration number when the 'if condition' triggers, that is,

$$\mathcal{K} \coloneqq \min_k \left\{ k \middle| k \sum_{t=0}^{k-1} \left\| (\sqrt{\mathbf{n}_t} + \varepsilon)^{1/2} \circ (\mathbf{y}_{t+1} - \mathbf{y}_t) \right\|^2 > R^2 \right\}.$$

Proposition 1. *Given $k \leq \mathcal{K}$ and $\beta \leq \varepsilon/\left(\sqrt{2}c_\infty + \varepsilon\right)$, we have:*

$$\left\| (\sqrt{\mathbf{n}_k} + \varepsilon)^{1/2} \circ (\mathbf{x}_k - \mathbf{y}_k) \right\| \leq R.$$

Proof. First of all, we let $\hat{\mathbf{n}}_k \coloneqq \left(\sqrt{\mathbf{n}_k} + \varepsilon\right)^{1/2}$. Due to Proposition 3, we have:

$$\left(\frac{\sqrt{\mathbf{n}_{k-1}} + \varepsilon}{\sqrt{\mathbf{n}_k} + \varepsilon} \right)_i \in \left[1 - \frac{\sqrt{2}\beta^2 c_\infty}{\varepsilon}, 1 + \frac{\sqrt{2}\beta^2 c_\infty}{\varepsilon} \right],$$

then, we get:

$$\hat{\mathbf{n}}_k \leq \left(1 - \frac{\sqrt{2}\beta^2 c_\infty}{\varepsilon} \right)^{-1/2} \hat{\mathbf{n}}_{k-1} \leq (1-\beta)^{-1/4} \hat{\mathbf{n}}_{k-1},$$

where we use the fact $\beta \leq \varepsilon/\left(2\sqrt{2}c_\infty + \varepsilon\right)$.For any $1 \leq k \leq \mathcal{K}$, we have:

$$\begin{aligned} &\|\hat{\mathbf{n}}_k \circ (\mathbf{y}_k - \mathbf{y}_{k-1})\|^2 \leq (1-\beta)^{-1/2} \|\hat{\mathbf{n}}_{k-1} \circ (\mathbf{y}_k - \mathbf{y}_{k-1})\|^2 \\ \leq &(1-\beta)^{-1} \sum_{t=1}^{k-1} \|\hat{\mathbf{n}}_t \circ (\mathbf{y}_{t+1} - \mathbf{y}_t)\|^2 \leq \frac{R^2}{k(1-\beta)}, \end{aligned}$$

hence, we can conclude that:

$$\|\hat{\mathbf{n}}_k \circ (\mathbf{y}_k - \mathbf{y}_{k-1})\|^2 \leq \frac{R^2}{k(1-\beta)}. \tag{16}$$

On the other hand, by Eq.(15), we have:

$$\mathbf{x}_{k+1} - \mathbf{y}_{k+1} = (1-\beta) \left[(\mathbf{y}_{k+1} - \mathbf{y}_k) + \frac{\boldsymbol{\eta}_k - \boldsymbol{\eta}_{k-1}}{\boldsymbol{\eta}_{k-1}} (\mathbf{x}_k - \mathbf{y}_k) \right],$$

and hence,

$$\begin{aligned} &\|\hat{\mathbf{n}}_k \circ (\mathbf{x}_k - \mathbf{y}_k)\| \leq (1-\beta) \left[\|\hat{\mathbf{n}}_k \circ (\mathbf{y}_k - \mathbf{y}_{k-1})\| + \left\| \frac{\boldsymbol{\eta}_{k-1} - \boldsymbol{\eta}_{k-2}}{\boldsymbol{\eta}_{k-2}} \right\|_\infty \|\hat{\mathbf{n}}_k \circ (\mathbf{x}_{k-1} - \mathbf{y}_{k-1})\| \right] \\ &\overset{(a)}{\leq} \sqrt{1-\beta} \frac{R}{\sqrt{k}} + (1-\beta) \frac{\sqrt{2}\beta^2 c_\infty}{\varepsilon} \left(1 - \frac{\sqrt{2}\beta^2 c_\infty}{\varepsilon} \right)^{-1/2} \|\hat{\mathbf{n}}_{k-1} \circ (\mathbf{x}_{k-1} - \mathbf{y}_{k-1})\| \\ &\leq \sqrt{1-\beta} \frac{R}{\sqrt{k}} + \beta (1-\beta)^{3/4} \|\hat{\mathbf{n}}_{k-1} \circ (\mathbf{x}_{k-1} - \mathbf{y}_{k-1})\| \\ &\leq \sqrt{1-\beta} R \left(\frac{1}{\sqrt{k}} + \frac{\beta(1-\beta)^{3/4}}{\sqrt{k-1}} + \cdots + \left(\beta(1-\beta)^{3/4} \right)^{k-1} \right) \\ &\overset{(b)}{\leq} \sqrt{1-\beta} R \left(\sum_{t=1}^{k-1} \frac{1}{t^2} \right)^{1/4} \left(\sum_{t=0}^{k} \left(\beta(1-\beta)^{3/4} \right)^{4t/3} \right)^{3/4} \overset{(c)}{<} R, \end{aligned}$$

where (a) comes from Eq.(16) and the proposition 3, (b) is the application of Hölder's inequality and (c) comes from the facts when $\beta \leq 1/2$:

$$\sum_{t=1}^{\infty} \frac{1}{t^2} = \frac{\pi^2}{6}, \quad \sqrt{1-\beta} \left(\sum_{t=0}^{k} \left(\beta(1-\beta)^{3/4} \right)^{4t/3} \right)^{3/4} \leq \left(\frac{(1-\beta)^{2/3}}{1 - \beta^{4/3}(1-\beta)} \right)^{3/4}.$$

□

B.4.3 Decrease of One Restart Cycle

Lemma 3. *Suppose that Assumptions 1-2 hold. Let* $R = \mathcal{O}(\epsilon^{0.5})$, $\beta = \mathcal{O}(\epsilon^2)$, $\eta = \mathcal{O}(\epsilon^{1.5})$, $\mathcal{K} \leq K = \mathcal{O}(\epsilon^{-2})$. *Then we have:*

$$\mathbb{E}\left(f(\mathbf{y}_{\mathcal{K}}) - f(\mathbf{x}_0)\right) = -\mathcal{O}(\epsilon^{1.5}). \tag{17}$$

Proof. Recall Eq.(15) and denote $\mathbf{g}_k^{full} \coloneqq \nabla f(\boldsymbol{\theta}_k)$ for convenience:

$$\begin{cases} \mathbf{y}_{k+1} = \mathbf{x}_k - \beta\boldsymbol{\eta}_k \circ \left(\mathbf{g}_k^{full} + \boldsymbol{\xi}_k\right) \\ \mathbf{x}_{k+1} - \mathbf{y}_{k+1} = (1-\beta)\left[(\mathbf{y}_{k+1} - \mathbf{y}_k) + \left(\dfrac{\boldsymbol{\eta}_k - \boldsymbol{\eta}_{k-1}}{\boldsymbol{\eta}_{k-1}} \circ (\mathbf{x}_k - \mathbf{y}_k)\right)\right], \end{cases} \tag{18}$$

In this proof, we let $\hat{\mathbf{n}}_k \coloneqq \left(\sqrt{\mathbf{n}_k} + \varepsilon\right)^{1/2}$, and hence $\boldsymbol{\eta}_k = \eta/\hat{\mathbf{n}}_k^2$. On one hand, we have:

$$\begin{aligned}
&\mathbb{E}(f(\mathbf{x}_k) - f(\mathbf{y}_k)) \leq \mathbb{E}\left(\langle \nabla f(\mathbf{y}_k), \mathbf{x}_k - \mathbf{y}_k\rangle + \frac{L}{2}\|\mathbf{x}_k - \mathbf{y}_k\|^2\right) \\
=&\mathbb{E}\left(\langle \mathbf{g}_k, \mathbf{x}_k - \mathbf{y}_k\rangle + \langle \nabla f(\mathbf{y}_k) - \nabla f(\mathbf{x}_k), \mathbf{x}_k - \mathbf{y}_k\rangle + \frac{L}{2}\|\mathbf{x}_k - \mathbf{y}_k\|^2\right) \\
\leq&\mathbb{E}\left(\langle \mathbf{g}_k, \mathbf{x}_k - \mathbf{y}_k\rangle + \frac{1}{2L}\|\nabla f(\mathbf{y}_k) - \nabla f(\mathbf{x}_k)\|^2 + \frac{L}{2}\|\mathbf{x}_k - \mathbf{y}_k\|^2 + \frac{L}{2}\|\mathbf{x}_k - \mathbf{y}_k\|^2\right) \\
\leq&\mathbb{E}\left(\langle \mathbf{g}_k, \mathbf{x}_k - \mathbf{y}_k\rangle + \frac{3L}{2}\|\mathbf{x}_k - \mathbf{y}_k\|^2\right) \\
=&\mathbb{E}\left(-\left\langle \frac{\mathbf{y}_{k+1} - \mathbf{x}_k}{\beta\boldsymbol{\eta}_k} + \boldsymbol{\xi}_k, \mathbf{x}_k - \mathbf{y}_k\right\rangle + \frac{3L}{2}\|\mathbf{x}_k - \mathbf{y}_k\|^2\right) \\
=&\mathbb{E}\left(\frac{1}{\eta\beta}\left\langle \hat{\mathbf{n}}_k^2 \circ (\mathbf{y}_{k+1} - \mathbf{x}_k), \mathbf{y}_k - \mathbf{x}_k\right\rangle + \frac{3L}{2}\|\mathbf{x}_k - \mathbf{y}_k\|^2\right) \\
\overset{(a)}{\leq}&\mathbb{E}\left(\frac{1}{2\eta\beta}\left(\|\hat{\mathbf{n}}_k \circ (\mathbf{y}_{k+1} - \mathbf{x}_k)\|^2 + \|\hat{\mathbf{n}}_k \circ (\mathbf{y}_k - \mathbf{x}_k)\|^2 - \|\hat{\mathbf{n}}_k \circ (\mathbf{y}_{k+1} - \mathbf{y}_k)\|^2\right) + \frac{3L}{2}\|\mathbf{x}_k - \mathbf{y}_k\|^2\right) \\
\overset{(b)}{\leq}&\mathbb{E}\left(\frac{1}{2\eta\beta}\left(\|\hat{\mathbf{n}}_k \circ (\mathbf{y}_{k+1} - \mathbf{x}_k)\|^2 - \|\hat{\mathbf{n}}_k \circ (\mathbf{y}_{k+1} - \mathbf{y}_k)\|^2\right) + \frac{1+\beta/2}{2\eta\beta}\|\hat{\mathbf{n}}_k \circ (\mathbf{y}_k - \mathbf{x}_k)\|^2\right)
\end{aligned} \tag{19}$$

where (a) comes from the following facts, and in (b), we use $3L\eta \leq \frac{\varepsilon}{2}$:

$$2\left\langle \hat{\mathbf{n}}_k^2 \circ (\mathbf{y}_{k+1} - \mathbf{x}_k), \mathbf{y}_k - \mathbf{x}_k\right\rangle = \|\hat{\mathbf{n}}_k \circ (\mathbf{y}_{k+1} - \mathbf{x}_k)\|^2 + \|\hat{\mathbf{n}}_k \circ (\mathbf{y}_k - \mathbf{x}_k)\|^2 - \|\hat{\mathbf{n}}_k \circ (\mathbf{y}_{k+1} - \mathbf{y}_k)\|^2.$$

On the other hand, by the L-smoothness condition, for $1 \leq k \leq \mathcal{K}$, we have:

$$\begin{aligned}
\mathbb{E}\left(f(\mathbf{y}_{k+1}) - f(\mathbf{x}_k)\right) \leq&\mathbb{E}\left(\langle \mathbf{g}_k, \mathbf{y}_{k+1} - \mathbf{x}_k\rangle + \frac{L}{2}\|\mathbf{y}_{k+1} - \mathbf{x}_k\|^2\right) \\
=&\mathbb{E}\left(-\left\langle \frac{\mathbf{y}_{k+1} - \mathbf{x}_k}{\beta\boldsymbol{\eta}_k} + \boldsymbol{\xi}_k, \mathbf{y}_{k+1} - \mathbf{x}_k\right\rangle + \frac{L}{2}\|\mathbf{y}_{k+1} - \mathbf{x}_k\|^2\right) \\
\overset{(a)}{\leq}&\mathbb{E}\left(-\frac{1}{\eta\beta}\|\hat{\mathbf{n}}_k \circ (\mathbf{y}_{k+1} - \mathbf{x}_k)\|^2 + \frac{L}{2}\|\mathbf{y}_{k+1} - \mathbf{x}_k\|^2\right) + \frac{\eta\beta\sigma^2}{\varepsilon} \\
\leq&\mathbb{E}\left(-\frac{1}{\eta\beta}\|\hat{\mathbf{n}}_k \circ (\mathbf{y}_{k+1} - \mathbf{x}_k)\|^2 + \frac{L}{2\varepsilon}\|\hat{\mathbf{n}}_k \circ (\mathbf{y}_{k+1} - \mathbf{x}_k)\|^2\right) + \frac{\eta\beta\sigma^2}{\varepsilon} \\
\leq&\mathbb{E}\left(-\frac{1}{2\eta\beta}\|\hat{\mathbf{n}}_k \circ (\mathbf{y}_{k+1} - \mathbf{x}_k)\|^2\right) + \frac{\eta\beta\sigma^2}{\varepsilon},
\end{aligned} \tag{20}$$

where (a) comes from the facts: $\mathbb{E}\left(\langle \boldsymbol{\xi}_k, \mathbf{y}_{k+1} - \mathbf{x}_k\rangle\right) = \mathbb{E}\left(\langle \boldsymbol{\xi}_k, \mathbf{x}_k - \beta\boldsymbol{\eta}_k \circ (\mathbf{g}_k + \boldsymbol{\xi}_k)\rangle\right) = \mathbb{E}\left(\langle \boldsymbol{\xi}_k, \beta\boldsymbol{\eta}_k \circ \boldsymbol{\xi}_k\rangle\right) \leq \frac{\eta\beta\sigma^2}{\varepsilon}$. and the last inequality is due to $L\eta \leq \varepsilon$. By combing Eq.(19) and

Eq.(20), we have:

$$\mathbb{E}\left(f(\mathbf{y}_{k+1})-f(\mathbf{y}_k)\right)\leq\mathbb{E}\left(-\frac{1}{2\eta\beta}\|\hat{\mathbf{n}}_k\circ(\mathbf{y}_{k+1}-\mathbf{y}_k)\|^2+\frac{1+\beta/2}{2\eta\beta}\|\hat{\mathbf{n}}_k\circ(\mathbf{y}_k-\mathbf{x}_k)\|^2\right)+\frac{\eta\beta\sigma^2}{\varepsilon}$$
$$\overset{(a)}{\leq}\mathbb{E}\left(-\frac{1}{2\eta\beta}\|\hat{\mathbf{n}}_k\circ(\mathbf{y}_{k+1}-\mathbf{y}_k)\|^2+\frac{1-\beta/2-\beta^2/2}{2\eta\beta}\|\hat{\mathbf{n}}_{k-1}\circ(\mathbf{y}_k-\mathbf{y}_{k-1})\|^2\right)+\frac{4\beta^2R^2c_\infty^2}{\eta\varepsilon^2}+\frac{\eta\beta\sigma^2}{\varepsilon},$$

where (a) comes from the following fact, and note that by Proposition 1 we already have $\hat{\mathbf{n}}_k\leq(1-\beta)^{-1/4}\hat{\mathbf{n}}_{k-1}$:

$$\begin{aligned}
&\|\hat{\mathbf{n}}_k\circ(\mathbf{x}_k-\mathbf{y}_k)\|^2\\
\leq&(1-\beta)^2\left[(1+\alpha)\|\hat{\mathbf{n}}_k\circ(\mathbf{y}_k-\mathbf{y}_{k-1})\|^2+(1+\frac{1}{\alpha})\hat{\beta}^2\|\hat{\mathbf{n}}_k\circ(\mathbf{x}_{k-1}-\mathbf{y}_{k-1})\|^2\right]\\
\leq&(1-\beta)^{3/2}\left[(1+\alpha)\|\hat{\mathbf{n}}_{k-1}\circ(\mathbf{y}_k-\mathbf{y}_{k-1})\|^2+(1+\frac{1}{\alpha})\hat{\beta}^2\|\hat{\mathbf{n}}_{k-1}\circ(\mathbf{x}_{k-1}-\mathbf{y}_{k-1})\|^2\right]\\
\leq&(1-\beta)\|\hat{\mathbf{n}}_{k-1}\circ(\mathbf{y}_k-\mathbf{y}_{k-1})\|^2+\frac{\hat{\beta}^2(1-\beta)^{3/2}}{1-(1-\beta)^{1/2}}\|\hat{\mathbf{n}}_{k-1}\circ(\mathbf{x}_{k-1}-\mathbf{y}_{k-1})\|^2\\
\leq&(1-\beta)\|\hat{\mathbf{n}}_{k-1}\circ(\mathbf{y}_k-\mathbf{y}_{k-1})\|^2+\frac{2\hat{\beta}^2}{\beta}\|\hat{\mathbf{n}}_{k-1}\circ(\mathbf{x}_{k-1}-\mathbf{y}_{k-1})\|^2\\
\leq&(1-\beta)\|\hat{\mathbf{n}}_{k-1}\circ(\mathbf{y}_k-\mathbf{y}_{k-1})\|^2+4\beta^3R^2c_\infty^2/\varepsilon^2,
\end{aligned}\tag{21}$$

where we let $\hat{\beta}:=\sqrt{2}\beta^2c_\infty/\varepsilon$, $\alpha=(1-\beta)^{-1/2}-1$, and the last inequality we use the results in Proposition 1. Summing over $k=2,\cdots,\mathcal{K}-1$, and note that $\mathbf{y}_1=\mathbf{x}_1$, and hence we have $\mathbb{E}\left(f(\mathbf{y}_2)-f(\mathbf{x}_1)\right)=\mathbb{E}\left(f(\mathbf{y}_2)-f(\mathbf{y}_1)\right)\leq\eta\beta\sigma c_\infty/\sqrt{\varepsilon}$ due to Eq. (20), then we get:

$$\mathbb{E}\left(f(\mathbf{y}_{\mathcal{K}})-f(\mathbf{y}_1)\right)\leq\mathbb{E}\left(-\frac{1}{4\eta}\sum_{t=1}^{\mathcal{K}-1}\|\hat{\mathbf{n}}_k\circ(\mathbf{y}_{t+1}-\mathbf{y}_t)\|^2\right)+\frac{4\mathcal{K}\beta^2R^2c_\infty^2}{\eta\varepsilon^2}+\frac{\mathcal{K}\eta\beta\sigma^2}{\varepsilon}.$$

On the other hand, similar to the results given in Eq.(20), we have:

$$\mathbb{E}\left(f(\mathbf{y}_1)-f(\mathbf{y}_0)\right)=\mathbb{E}\left(f(\mathbf{x}_1)-f(\mathbf{x}_0)\right)\leq\mathbb{E}\left(-\frac{1}{2\eta}\|\hat{\mathbf{n}}_k\circ(\mathbf{y}_1-\mathbf{y}_0)\|^2\right)+\frac{\eta\sigma^2}{\varepsilon}.$$

Therefore, using $\beta\mathcal{K}=\mathcal{O}(1)$ and the restart condition $\mathcal{K}\sum_{t=0}^{\mathcal{K}-1}\left\|(\sqrt{\mathbf{n}_t}+\varepsilon)^{1/2}\circ(\mathbf{y}_{t+1}-\mathbf{y}_t)\right\|^2\geq R^2$, we can get:

$$\mathbb{E}\left(f(\mathbf{y}_{\mathcal{K}})-f(\mathbf{y}_0)\right)\leq\mathbb{E}\left(-\frac{1}{4\eta}\sum_{t=0}^{\mathcal{K}-1}\|\hat{\mathbf{n}}_k\circ(\mathbf{y}_{k+1}-\mathbf{y}_k)\|^2\right)+\frac{4\mathcal{K}\beta^2R^2c_\infty^2}{\eta\varepsilon^2}+\frac{(\mathcal{K}\beta+1)\eta\sigma^2}{\varepsilon}$$
$$\leq-\frac{R^2}{4\mathcal{K}\eta}+\frac{4\mathcal{K}\beta^2R^2c_\infty^2}{\eta\varepsilon^2}+\frac{(\mathcal{K}\beta+1)\eta\sigma^2}{\varepsilon}=-\mathcal{O}\left(\frac{R^2}{\mathcal{K}\eta}-\frac{\beta R^2}{\eta}-\eta\right)=-\mathcal{O}\left(\epsilon^{1.5}\right).$$

Now, we finish the proof of this claim. □

B.4.4 Gradient in the last Restart Cycle

Before showing the main results, we first provide several definitions. Note that, for any $k<\mathcal{K}$ we already have:

$$(\varepsilon)^{1/2}\|\mathbf{y}_k-\mathbf{y}_0\|\leq(\varepsilon)^{1/2}\sqrt{k\sum_{t=0}^{k-1}\|\mathbf{y}_{t+1}-\mathbf{y}_t\|^2}\leq R.$$

and we have:

$$\mathbb{E}\left(\|\mathbf{x}_k-\mathbf{x}_0\|\right)\leq\mathbb{E}\left(\|\mathbf{y}_k-\mathbf{x}_k\|+\|\mathbf{y}_k-\mathbf{x}_0\|\right)\leq\frac{2R}{\varepsilon^{1/2}},\tag{22}$$

where we utilize the results from Proposition 1. For each epoch, denote $\mathbf{H}:=\nabla^2f(\mathbf{x}_0)$. We then define:

$$h(\mathbf{y}):=\left\langle\mathbf{g}_0^{full},\mathbf{y}-\mathbf{x}_0\right\rangle+\frac{1}{2}(\mathbf{y}-\mathbf{x}_0)^\top\mathbf{H}(\mathbf{y}-\mathbf{x}_0).$$

Recall the Eq. (15):

$$\begin{cases} \mathbf{y}_{k+1} = \mathbf{x}_k - \beta \boldsymbol{\eta}_k \circ \left(\mathbf{g}_k^{full} + \boldsymbol{\xi}_k \right) = \mathbf{x}_k - \beta \boldsymbol{\eta}_k \circ \left(\nabla h(\mathbf{x}_k) + \boldsymbol{\delta}_k + \boldsymbol{\xi}_k \right) \\ \mathbf{x}_{k+1} - \mathbf{y}_{k+1} = (1-\beta) \left[(\mathbf{y}_{k+1} - \mathbf{y}_k) + \left(\frac{\boldsymbol{\eta}_k - \boldsymbol{\eta}_{k-1}}{\boldsymbol{\eta}_{k-1}} \circ (\mathbf{x}_k - \mathbf{y}_k) \right) \right], \end{cases} \tag{23}$$

where we let $\boldsymbol{\delta}_k \coloneqq \mathbf{g}_k^{full} - \nabla h(\mathbf{x}_k)$, and we can get that:

$$\begin{aligned} &\mathbb{E}\left(\|\boldsymbol{\delta}_k\| \right) = \mathbb{E}\left(\left\| \mathbf{g}_k^{full} - \mathbf{g}_0^{full} - \mathbf{H}(\mathbf{x}_k - \mathbf{x}_0) \right\| \right) \\ =& \mathbb{E}\left(\left\| \left(\int_0^1 \nabla^2 h(\mathbf{x}_0 + t(\mathbf{x}_k - \mathbf{x}_0)) - \mathbf{H} \right) (\mathbf{x}_k - \mathbf{x}_0) dt \right\| \right) \leq \frac{\rho}{2} \mathbb{E}\left(\|\mathbf{x}_k - \mathbf{x}_0\|^2 \right) \leq \frac{2\rho R^2}{\varepsilon}. \end{aligned} \tag{24}$$

Iterations in Eq.(23) can be viewed as applying the proposed optimizer to the quadratic approximation $h(\mathbf{x})$ with the gradient error δ_k, which is in the order of $\mathcal{O}\left(\rho R^2/\varepsilon\right)$.

Lemma 4. *Suppose that Assumptions 1-3 hold. Let* $B = \mathcal{O}\left(\epsilon^{0.5}\right)$, $\beta = \mathcal{O}\left(\epsilon^2\right)$, $\eta = \mathcal{O}\left(\epsilon^{1.5}\right)$, $\mathcal{K} \leq K = \mathcal{O}\left(\epsilon^{-2}\right)$. *Then we have:*

$$\mathbb{E}\left(\|\nabla f(\bar{\mathbf{x}})\| \right) = \mathcal{O}(\epsilon), \quad \textit{where } \bar{\mathbf{x}} \coloneqq \frac{1}{K_0 - 1} \sum_{k=1}^{K_0} \mathbf{x}_k.$$

Proof. Since $h(\cdot)$ is quadratic, then we have:

$$
\begin{aligned}
&\mathbb{E}\left(\|\nabla h(\bar{\mathbf{x}})\|\right)=\mathbb{E}\left(\left\|\frac{1}{K_0-1}\sum_{k=1}^{K_0}\nabla h(\mathbf{x}_k)\right\|\right)\\
=&\frac{1}{K_0-1}\,\mathbb{E}\left\|\sum_{k=1}^{K_0}(\beta\boldsymbol{\eta}_k)^{-1}\circ(\mathbf{y}_{k+1}-\mathbf{x}_k)+\boldsymbol{\xi}_k+\boldsymbol{\delta}_k\right\|\\
\leq&\frac{1}{(K_0-1)\beta}\,\mathbb{E}\left\|\sum_{k=1}^{K_0}(\beta\boldsymbol{\eta}_k)^{-1}\circ(\mathbf{y}_{k+1}-\mathbf{x}_k)\right\|+\frac{1}{(K_0-1)}\,\mathbb{E}\left\|\sum_{k=1}^{K_0}\boldsymbol{\xi}_k\right\|+\frac{1}{(K_0-1)}\,\mathbb{E}\left\|\sum_{k=1}^{K_0}\boldsymbol{\delta}_k\right\|\\
\overset{(a)}{\leq}&\frac{1}{(K_0-1)\beta}\,\mathbb{E}\left\|\sum_{k=1}^{K_0}(\boldsymbol{\eta}_k)^{-1}\circ(\mathbf{y}_{k+1}-\mathbf{x}_k)\right\|+\frac{\sigma}{\sqrt{K_0-1}}+\frac{2\rho R^2}{\varepsilon}\\
=&\frac{1}{(K_0-1)\beta}\,\mathbb{E}\left\|\sum_{k=1}^{K_0}\frac{\mathbf{y}_{k+1}-\mathbf{y}_k-(1-\beta)(\mathbf{y}_k-\mathbf{y}_{k-1})}{\boldsymbol{\eta}_k}-(1-\beta)\frac{\boldsymbol{\eta}_{k-1}-\boldsymbol{\eta}_{k-2}}{\boldsymbol{\eta}_{k-2}\boldsymbol{\eta}_k}(\mathbf{x}_{k-1}-\mathbf{y}_{k-1})\right\|\\
&+\frac{\sigma}{\sqrt{K_0-1}}+\frac{2\rho R^2}{\varepsilon}\\
\overset{(b)}{\leq}&\frac{1}{(K_0-1)\beta}\,\mathbb{E}\left\|\sum_{k=1}^{K_0}\frac{\mathbf{y}_{k+1}-\mathbf{y}_k-(1-\beta)(\mathbf{y}_k-\mathbf{y}_{k-1})}{\boldsymbol{\eta}_k}\right\|+\frac{2\beta c_\infty^{1.5}R}{\eta\varepsilon}+\frac{\sigma}{\sqrt{K_0-1}}+\frac{2\rho R^2}{\varepsilon}\\
\overset{(c)}{\leq}&\frac{1}{(K_0-1)\beta}\,\mathbb{E}\left\|\sum_{k=1}^{K_0}\left(\frac{\mathbf{y}_{k+1}-\mathbf{y}_k}{\boldsymbol{\eta}_k}-\frac{(1-\beta)(\mathbf{y}_k-\mathbf{y}_{k-1})}{\boldsymbol{\eta}_{k-1}}\right)\right\|+\frac{4\beta c_\infty^{1.5}R}{\eta\varepsilon}+\frac{\sigma}{\sqrt{K_0-1}}+\frac{2\rho R^2}{\varepsilon}\\
\leq&\frac{1}{(K_0-1)\beta}\,\mathbb{E}\left\|\frac{\mathbf{y}_{K_0}-\mathbf{y}_{K_0-1}}{\boldsymbol{\eta}_{K_0}}\right\|+\frac{1}{(K_0-1)}\,\mathbb{E}\left\|\sum_{k=1}^{K_0-1}\frac{\mathbf{y}_{k+1}-\mathbf{y}_k}{\boldsymbol{\eta}_k}\right\|+\frac{4\beta c_\infty^{1.5}R}{\eta\varepsilon}\\
&+\frac{\sigma}{\sqrt{K_0-1}}+\frac{2\rho R^2}{\varepsilon}\\
\overset{(d)}{\leq}&\frac{1}{(K_0-1)}\,\mathbb{E}\left\|\sum_{k=1}^{K_0}\frac{\mathbf{y}_{k+1}-\mathbf{y}_k}{\boldsymbol{\eta}_k}\right\|+\frac{4R\sqrt{c_\infty}}{\beta\eta K^2}+\frac{4\beta c_\infty^{1.5}R}{\eta\varepsilon}+\frac{\sigma}{\sqrt{K_0-1}}+\frac{2\rho R^2}{\varepsilon}\\
\leq&\frac{\sqrt{2c_\infty}}{\eta K}\,\mathbb{E}\left\|\sum_{k=1}^{K_0}\left(\sqrt{\mathbf{n}_k}+\varepsilon\right)^{1/2}\circ(\mathbf{y}_{k+1}-\mathbf{y}_k)\right\|+\frac{4R\sqrt{c_\infty}}{\beta\eta K^2}+\frac{4\beta c_\infty^{1.5}B}{\eta\varepsilon}+\frac{\sigma}{\sqrt{K_0-1}}+\frac{2\rho R^2}{\varepsilon}\\
\leq&\frac{\sqrt{2c_\infty}R}{\eta K}+\frac{4R\sqrt{c_\infty}}{\beta\eta K^2}+\frac{4\beta c_\infty^{1.5}R}{\eta\varepsilon}+\frac{\sigma}{\sqrt{K_0-1}}+\frac{2\rho R^2}{\varepsilon}=\mathcal{O}\left(\frac{R}{\eta K}+\frac{\beta R}{\eta}+\frac{1}{\sqrt{K}}+R^2\right)=\mathcal{O}(\epsilon),
\end{aligned}
$$

where (a) is due to the independence of $\boldsymbol{\xi}_k$'s and Eq.(24), (b) comes from Propositions 1 and 2:

$$
\begin{aligned}
&\left\|\frac{\boldsymbol{\eta}_{k-1}-\boldsymbol{\eta}_{k-2}}{\boldsymbol{\eta}_{k-2}\boldsymbol{\eta}_k}(\mathbf{x}_{k-1}-\mathbf{y}_{k-1})\right\|\leq\frac{\sqrt{\mathbf{n}_k}+\varepsilon}{\eta\left(\sqrt{\mathbf{n}_{k-1}}+\varepsilon\right)^{1/2}}\left\|\frac{\boldsymbol{\eta}_{k-1}-\boldsymbol{\eta}_{k-2}}{\boldsymbol{\eta}_{k-2}}\right\|_\infty\|\hat{\mathbf{n}}_{k-1}\circ(\mathbf{x}_{k-1}-\mathbf{y}_{k-1})\|\\
\leq&\frac{\left(\sqrt{\mathbf{n}_k}+\varepsilon\right)^{1/2}}{\eta}\frac{\sqrt{2}\beta^2c_\infty}{\varepsilon}\left(1-\frac{\sqrt{2}\beta^2c_\infty}{\varepsilon}\right)^{-1/2}R\\
\leq&\frac{\left(c_\infty+\varepsilon\right)^{1/2}}{\eta}\frac{\sqrt{2}\beta^2c_\infty}{\varepsilon}\frac{R}{(1-\beta)^{1/4}}\leq\left(\frac{1}{1-\beta}\right)^{1/4}\frac{2\beta^2c_\infty^{1.5}R}{\eta\varepsilon},
\end{aligned}
$$

we use the following bounds in (c):

$$\left\|\frac{(\mathbf{y}_k-\mathbf{y}_{k-1})}{\boldsymbol{\eta}_{k-1}}-\frac{(\mathbf{y}_k-\mathbf{y}_{k-1})}{\boldsymbol{\eta}_k}\right\|=\left\|\frac{\boldsymbol{\eta}_k-\boldsymbol{\eta}_{k-1}}{\boldsymbol{\eta}_{k-1}\boldsymbol{\eta}_k}(\mathbf{y}_k-\mathbf{y}_{k-1})\right\|$$
$$\leq\frac{\left(\sqrt{\mathbf{n}_{k-1}}+\varepsilon\right)^{1/2}}{\eta}\left\|\frac{\boldsymbol{\eta}_k-\boldsymbol{\eta}_{k-1}}{\boldsymbol{\eta}_k}\right\|_\infty\left\|\left(\sqrt{\mathbf{n}_{k-1}}+\varepsilon\right)^{1/2}\circ(\mathbf{y}_k-\mathbf{y}_{k-1})\right\|$$
$$\leq\frac{\left(\sqrt{\mathbf{n}_{k-1}}+\varepsilon\right)^{1/2}}{\eta}\frac{\sqrt{2}\beta^2c_\infty}{\varepsilon}\frac{R}{k}\leq\frac{(c_\infty+\varepsilon)^{1/2}}{\eta}\frac{\sqrt{2}\beta^2c_\infty}{\varepsilon}\frac{R}{k}\leq\frac{2\beta^2c_\infty^{1.5}R}{\eta\varepsilon k},$$

(d) is implied by $K_0=\operatorname{argmin}_{\lfloor\frac{K}{2}\rfloor\leq k\leq K-1}\left\|\left(\sqrt{\mathbf{n}_k}+\varepsilon\right)^{1/2}\circ(\mathbf{y}_{k+1}-\mathbf{y}_k)\right\|$ and restart condition:

$$\left\|\frac{\mathbf{y}_{K_0}-\mathbf{y}_{K_0-1}}{\boldsymbol{\eta}_{K_0}}\right\|^2\leq\frac{\sqrt{\mathbf{n}_{K_0}}+\varepsilon}{\eta^2}\left\|\left(\sqrt{\mathbf{n}_{K_0}}+\varepsilon\right)^{1/2}\circ(\mathbf{y}_{K_0}-\mathbf{y}_{K_0-1})\right\|^2$$
$$\left\|\left(\sqrt{\mathbf{n}_{K_0}}+\varepsilon\right)^{1/2}\circ(\mathbf{y}_{K_0}-\mathbf{y}_{K_0-1})\right\|^2\leq\frac{1}{K-\lfloor K/2\rfloor}\sum_{k=\lfloor K/2\rfloor}^{K-1}\left\|\left(\sqrt{\mathbf{n}_k}+\varepsilon\right)^{1/2}\circ(\mathbf{y}_{k+1}-\mathbf{y}_k)\right\|^2$$
$$\leq\frac{1}{K-\lfloor K/2\rfloor}\sum_{k=1}^{K}\left\|\left(\sqrt{\mathbf{n}_k}+\varepsilon\right)^{1/2}\circ(\mathbf{y}_{k+1}-\mathbf{y}_k)\right\|^2\leq\frac{1}{K-\lfloor K/2\rfloor}\frac{R^2}{K}\leq\frac{2R^2}{K^2}.$$

Finally, we have:

$$\mathbb{E}\left(\|\nabla f(\bar{\mathbf{x}})\|\right)=\mathbb{E}\left(\|\nabla h(\bar{\mathbf{x}})\|\right)+\mathbb{E}\left(\|\nabla f(\bar{\mathbf{x}})-\nabla h(\bar{\mathbf{x}})\|\right)=\mathcal{O}(\epsilon)+\frac{2\rho R^2}{\varepsilon}=\mathcal{O}(\epsilon),$$

where we use the results from Eq.(24), namely:

$$\mathbb{E}\left(\|\nabla f(\bar{\mathbf{x}})-\nabla h(\bar{\mathbf{x}})\|\right)=\mathbb{E}\left(\left\|\nabla f(\bar{\mathbf{x}})-\mathbf{g}_0^{full}-\mathbf{H}(\bar{\mathbf{x}}-\mathbf{x}_0)\right\|\right)\leq\frac{\rho}{2}\mathbb{E}\left(\|\bar{\mathbf{x}}-\mathbf{x}_0\|^2\right),$$

and we also note that, by Eq.(22):

$$\mathbb{E}\|\bar{\mathbf{x}}-\mathbf{x}_0\|\leq\frac{1}{K_0-1}\sum_{k=1}^{K_0}\mathbb{E}\|\mathbf{x}_k-\mathbf{x}_0\|\leq\frac{2R}{\varepsilon^{1/2}}.$$

□

B.4.5 Proof for Main Theorem

Theorem 2. *Suppose that Assumptions 1-3 hold. Let $B=\mathcal{O}(\epsilon^{0.5})$, $\beta=\mathcal{O}(\epsilon^2)$, $\eta=\mathcal{O}(\epsilon^{1.5})$, $\mathcal{K}\leq K=\mathcal{O}(\epsilon^{-2})$. Then Algorithm 1 find an ϵ-approximate first-order stationary point within at most $\mathcal{O}(\epsilon^{-3.5})$ iterations. Namely, we have:*

$$\mathbb{E}\left(f(\mathbf{y}_{\mathcal{K}})-f(\mathbf{x}_0)\right)=-\mathcal{O}(\epsilon^{1.5}),\quad\mathbb{E}\left(\|\nabla f(\bar{\mathbf{x}})\|\right)=\mathcal{O}(\epsilon).$$

Proof. Note that at the beginning of each restart cycle in Algorithm 2, we set $\mathbf{x}_0$ to be the last iterate $\mathbf{x}_{\mathcal{K}}$ in the previous restart cycle. Due to Lemma 3, we already have:

$$\mathbb{E}\left(f(\mathbf{y}_{\mathcal{K}})-f(\mathbf{x}_0)\right)=-\mathcal{O}(\epsilon^{1.5}).$$

Summing this inequality over all cycles, say N total restart cycles, we have:

$$\min_{\mathbf{x}}f(\mathbf{x})-f(\mathbf{x}_{\text{init}})=-\mathcal{O}(N\epsilon^{1.5}),$$

Hence, the Algorithm 2 terminates within at most $\mathcal{O}(\epsilon^{-1.5}\Delta_f)$ restart cycles, where $\Delta_f:=f(\mathbf{x}_{\text{init}})-\min_{\mathbf{x}}f(\mathbf{x})$. Note that each cycle contain at most $K=\mathcal{O}(\epsilon^{-2})$ iteration step, therefore, the total iteration number must be less than $\mathcal{O}(\epsilon^{-3.5}\Delta_f)$.

On the other hand, by Lemma 4, in the last restart cycle, we have:

$$\mathbb{E}\left(\|\nabla f(\bar{\mathbf{x}})\|\right)=\mathcal{O}(\epsilon).$$

Now, we obtain the final conclusion for the theorem. □

B.5 Auxiliary Lemmas

Proposition 2. *If Assumption 2 holds. We have:*

$$\|\mathbf{m}_k\|_\infty \leq c_\infty, \quad \|\mathbf{n}_k\|_\infty \leq c_\infty^2.$$

Proof. By the definition of $\mathbf{m}_k$, we can have that:

$$\mathbf{m}_k = \sum_{t=0}^{k} c_{k,t}\mathbf{g}_t,$$

where

$$c_{k,t} = \begin{cases} \beta_1(1-\beta_1)^{(k-t)} & \text{when } t > 0, \\ (1-\beta_1)^k & \text{when } t = 0. \end{cases}$$

Similar, we also have:

$$\mathbf{n}_k = \sum_{t=0}^{k} c'_{k,t}(\mathbf{g}_t + (1-\beta_2)(\mathbf{g}_t - \mathbf{g}_{t-1}))^2,$$

where

$$c'_{k,t} = \begin{cases} \beta_3(1-\beta_3)^{(k-t)} & \text{when } t > 0, \\ (1-\beta_3)^k & \text{when } t = 0. \end{cases}$$

If is obvious that:

$$\sum_{t=0}^{k} c_{k,t} = 1, \quad \sum_{t=0}^{k} c'_{k,t} = 1,$$

hence, we get:

$$\|\mathbf{m}_k\|_\infty \leq \sum_{t=0}^{k} c_{k,t}\|\mathbf{g}_t\|_\infty,$$

$$\|\mathbf{n}_k\|_\infty \leq \sum_{t=0}^{k} c'_{k,t}\|\mathbf{g}_t + (1-\beta_2)(\mathbf{g}_t - \mathbf{g}_{t-1})\|_\infty^2 \leq c_\infty^2.$$

□

Proposition 3. *If Assumption 2 holds, we have:*

$$\left\| \frac{\boldsymbol{\eta}_k - \boldsymbol{\eta}_{k-1}}{\boldsymbol{\eta}_{k-1}} \right\|_\infty \leq \frac{\sqrt{2}\beta_3 c_\infty}{\varepsilon}.$$

Proof. Give any index $i \in [d]$ and the definitions of $\boldsymbol{\eta}_k$, we have:

$$\left| \left(\frac{\boldsymbol{\eta}_k - \boldsymbol{\eta}_{k-1}}{\boldsymbol{\eta}_{k-1}} \right)_i \right| = \left| \left(\frac{\sqrt{\mathbf{n}_{k-1}} + \varepsilon}{\sqrt{\mathbf{n}_k} + \varepsilon} \right)_i - 1 \right| = \left| \left(\frac{\sqrt{\mathbf{n}_{k-1}} - \sqrt{\mathbf{n}_k}}{\sqrt{\mathbf{n}_k} + \varepsilon} \right)_i \right|.$$

Note that, by the definition of $\mathbf{n}_k$, we have:

$$\left| \left(\frac{\sqrt{\mathbf{n}_{k-1}} - \sqrt{\mathbf{n}_k}}{\sqrt{\mathbf{n}_k} + \varepsilon} \right)_i \right| \leq \left| \left(\frac{\sqrt{|\mathbf{n}_{k-1} - \mathbf{n}_k|}}{\sqrt{\mathbf{n}_k} + \varepsilon} \right)_i \right|$$

$$= \beta_3 \left(\frac{\sqrt{\left|\mathbf{n}_{k-1} - (\mathbf{g}_k + (1-\beta_2)(\mathbf{g}_k - \mathbf{g}_{k-1}))^2\right|}}{\sqrt{\mathbf{n}_k} + \varepsilon} \right)_i \leq \frac{\sqrt{2}\beta_3 c_\infty}{\varepsilon},$$

hence, we have:

$$\left| \left(\frac{\boldsymbol{\eta}_k - \boldsymbol{\eta}_{k-1}}{\boldsymbol{\eta}_{k-1}} \right)_i \right| \in \left[0, \frac{\sqrt{2}\beta_3 c_\infty}{\varepsilon} \right].$$

We finish the proof. □

Lemma 5. *Consider a moving average sequence:*

$$\mathbf{m}_k = (1-\beta)\mathbf{m}_{k-1} + \beta \mathbf{g}_k,$$

where we note that:

$$\mathbf{g}_k = \mathbb{E}_{\boldsymbol{\zeta}}[\nabla f(\boldsymbol{\theta}_k, \boldsymbol{\zeta})] + \boldsymbol{\xi}_k,$$

and we denote $\mathbf{g}_k^{full} \coloneqq E_{\boldsymbol{\zeta}}[\nabla f(\boldsymbol{\theta}_k, \boldsymbol{\zeta})]$ *for convenience. Then we have:*

$$\mathbb{E}\Big(\Big\|\mathbf{m}_k - \mathbf{g}_k^{full}\Big\|^2\Big) \leq (1-\beta)\mathbb{E}\Big(\Big\|\mathbf{m}_{k-1} - \mathbf{g}_{k-1}^{full}\Big\|^2\Big) + \frac{(1-\beta)^2 L^2}{\beta}\mathbb{E}\Big(\|\boldsymbol{\theta}_{k-1} - \boldsymbol{\theta}_k\|^2\Big) + \beta^2\sigma^2.$$

Proof. Note that, we have:

$$\begin{aligned}
\mathbf{m}_k - \mathbf{g}_k^{full} =& (1-\beta)\Big(\mathbf{m}_{k-1} - \mathbf{g}_{k-1}^{full}\Big) + (1-\beta)\mathbf{g}_{k-1}^{full} - \mathbf{g}_k^{full} + \beta \mathbf{g}_k \\
=& (1-\beta)\Big(\mathbf{m}_{k-1} - \mathbf{g}_{k-1}^{full}\Big) + (1-\beta)\Big(\mathbf{g}_{k-1}^{full} - \mathbf{g}_k^{full}\Big) + \beta\Big(\mathbf{g}_k - \mathbf{g}_k^{full}\Big).
\end{aligned}$$

Then, take expectation on both sides:

$$\begin{aligned}
&\mathbb{E}\Big(\Big\|\mathbf{m}_k - \mathbf{g}_k^{full}\Big\|^2\Big) \\
=&(1-\beta)^2\mathbb{E}\Big(\Big\|\mathbf{m}_{k-1} - \mathbf{g}_{k-1}^{full}\Big\|^2\Big) + (1-\beta)^2\mathbb{E}\Big(\Big\|\mathbf{g}_{k-1}^{full} - \mathbf{g}_k^{full}\Big\|^2\Big) + \beta^2\sigma^2 + \\
&2(1-\beta)^2\mathbb{E}\Big(\Big\langle \mathbf{m}_{k-1} - \mathbf{g}_{k-1}^{full}, \mathbf{g}_{k-1}^{full} - \mathbf{g}_k^{full}\Big\rangle\Big) \\
\leq&\Big((1-\beta)^2 + (1-\beta)^2 a\Big)\mathbb{E}\Big(\Big\|\mathbf{m}_{k-1} - \mathbf{g}_{k-1}^{full}\Big\|^2\Big) + \\
&\Big(1 + \frac{1}{a}\Big)(1-\beta)^2\mathbb{E}\Big(\Big\|\mathbf{g}_{k-1}^{full} - \mathbf{g}_k^{full}\Big\|^2\Big) + \beta^2\sigma^2 \\
\overset{(a)}{\leq}&(1-\beta)\mathbb{E}\Big(\Big\|\mathbf{m}_{k-1} - \mathbf{g}_{k-1}^{full}\Big\|^2\Big) + \frac{(1-\beta)^2}{\beta}\mathbb{E}\Big(\Big\|\mathbf{g}_{k-1}^{full} - \mathbf{g}_k^{full}\Big\|^2\Big) + \beta^2\sigma^2 \\
\leq&(1-\beta)\mathbb{E}\Big(\Big\|\mathbf{m}_{k-1} - \mathbf{g}_{k-1}^{full}\Big\|^2\Big) + \frac{(1-\beta)^2 L^2}{\beta}\mathbb{E}\Big(\|\boldsymbol{\theta}_{k-1} - \boldsymbol{\theta}_k\|^2\Big) + \beta^2\sigma^2,
\end{aligned}$$

where for (a), we set $a = \frac{\beta}{1-\beta}$. □

Lemma 6. *Consider a moving average sequence:*

$$\mathbf{v}_k = (1-\beta)\mathbf{v}_{k-1} + \beta(\mathbf{g}_k - \mathbf{g}_{k-1}),$$

where we note that:

$$\mathbf{g}_k = \mathbb{E}_{\boldsymbol{\zeta}}[\nabla f(\boldsymbol{\theta}_k, \boldsymbol{\zeta})] + \boldsymbol{\xi}_k,$$

and we denote $\mathbf{g}_k^{full} \coloneqq E_{\boldsymbol{\zeta}}[f(\boldsymbol{\theta}_k, \boldsymbol{\zeta})]$ *for convenience. Then we have:*

$$\mathbb{E}\Big(\|\mathbf{v}_k\|^2\Big) \leq (1-\beta)\mathbb{E}\Big(\|\mathbf{v}_{k-1}\|^2\Big) + 2\beta\mathbb{E}\Big(\Big\|\mathbf{g}_k^{full} - \mathbf{g}_{k-1}^{full}\Big\|^2\Big) + 3\beta^2\sigma^2.$$

Proof. Take expectation on both sides:

$$\begin{aligned}
&\mathbb{E}\Big(\|\mathbf{v}_k\|^2\Big) = (1-\beta)^2\mathbb{E}\Big(\|\mathbf{v}_{k-1}\|^2\Big) + \beta^2\mathbb{E}\Big(\|\mathbf{g}_k - \mathbf{g}_{k-1}\|^2\Big) + 2\beta(1-\beta)\mathbb{E}(\langle \mathbf{v}_{k-1}, \mathbf{g}_k - \mathbf{g}_{k-1}\rangle) \\
\overset{(a)}{=}&(1-\beta)^2\mathbb{E}\Big(\|\mathbf{v}_{k-1}\|^2\Big) + \beta^2\mathbb{E}\Big(\|\mathbf{g}_k - \mathbf{g}_{k-1}\|^2\Big) + 2\beta(1-\beta)\mathbb{E}\Big(\Big\langle \mathbf{v}_{k-1}, \mathbf{g}_k^{full} - \mathbf{g}_{k-1}\Big\rangle\Big) \\
\overset{(b)}{\leq}&(1-\beta)^2\mathbb{E}\Big(\|\mathbf{v}_{k-1}\|^2\Big) + 2\beta^2\mathbb{E}\Big(\Big\|\mathbf{g}_k^{full} - \mathbf{g}_{k-1}^{full}\Big\|^2\Big) + 2\beta(1-\beta)\mathbb{E}\Big(\Big\langle \mathbf{v}_{k-1}, \mathbf{g}_k^{full} - \mathbf{g}_{k-1}\Big\rangle\Big) + 3\beta^2\sigma^2 \\
\overset{(c)}{\leq}&(1-\beta)^2\mathbb{E}\Big(\|\mathbf{v}_{k-1}\|^2\Big) + 2\beta^2\mathbb{E}\Big(\Big\|\mathbf{g}_k^{full} - \mathbf{g}_{k-1}^{full}\Big\|^2\Big) + 2\beta(1-\beta)\mathbb{E}\Big(\Big\langle \mathbf{v}_{k-1}, \mathbf{g}_k^{full} - \mathbf{g}_{k-1}^{full}\Big\rangle\Big) + 3\beta^2\sigma^2 \\
\overset{(d)}{\leq}&(1-\beta)\mathbb{E}\Big(\|\mathbf{v}_{k-1}\|^2\Big) + 2\beta\mathbb{E}\Big(\Big\|\mathbf{g}_k^{full} - \mathbf{g}_{k-1}^{full}\Big\|^2\Big) + 3\beta^2\sigma^2,
\end{aligned}$$

where for (a), we utilize the independence between $\mathbf{g}_k$ and $\mathbf{v}_{k-1}$, while for (b):

$$\mathbb{E}\Big(\|\mathbf{g}_k - \mathbf{g}_{k-1}\|^2\Big) \leq \mathbb{E}\bigg(\Big\|\mathbf{g}_k - \mathbf{g}_k^{full}\Big\|^2\bigg) + 2\mathbb{E}\bigg(\Big\|\mathbf{g}_{k-1}^{full} - \mathbf{g}_{k-1}\Big\|^2\bigg) + 2\mathbb{E}\bigg(\Big\|\mathbf{g}_k^{full} - \mathbf{g}_{k-1}^{full}\Big\|^2\bigg),$$

for (c), we know:

$$\begin{aligned}
&\mathbb{E}\Big(\Big\langle \mathbf{v}_{k-1}, \mathbf{g}_{k-1}^{full} - \mathbf{g}_{k-1}\Big\rangle\Big) = \mathbb{E}\Big(\Big\langle (1-\beta)\mathbf{v}_{k-2} + \beta(\mathbf{g}_{k-1} - \mathbf{g}_{k-2}), \mathbf{g}_{k-1}^{full} - \mathbf{g}_{k-1}\Big\rangle\Big) \\
=&\mathbb{E}\Big(\Big\langle (1-\beta)\mathbf{v}_{k-2} - \beta\mathbf{g}_{k-2}, \mathbf{g}_{k-1}^{full} - \mathbf{g}_{k-1}\Big\rangle\Big) + \beta\mathbb{E}\Big(\Big\langle \mathbf{g}_{k-1} - \mathbf{g}_{k-1}^{full} + \mathbf{g}_{k-1}^{full}, \mathbf{g}_{k-1}^{full} - \mathbf{g}_{k-1}\Big\rangle\Big) \\
=&-\beta\mathbb{E}\Big(\Big\|\mathbf{g}_{k-1}^{full} - \mathbf{g}_{k-1}\Big\|^2\Big),
\end{aligned}$$

and thus $\mathbb{E}\Big(\Big\langle \mathbf{v}_{k-1}, \mathbf{g}_k^{full} - \mathbf{g}_{k-1}\Big\rangle\Big) = \mathbb{E}\Big(\Big\langle \mathbf{v}_{k-1}, \mathbf{g}_k^{full} - \mathbf{g}_{k-1}^{full}\Big\rangle\Big) - \beta\mathbb{E}\Big(\Big\|\mathbf{g}_{k-1}^{full} - \mathbf{g}_{k-1}\Big\|^2\Big)$. Finally, for (d), we use:

$$2\mathbb{E}\Big(\Big\langle \mathbf{v}_{k-1}, \mathbf{g}_k^{full} - \mathbf{g}_{k-1}^{full}\Big\rangle\Big) \leq \mathbb{E}\Big(\|\mathbf{v}_{k-1}\|^2\Big) + \mathbb{E}\bigg(\Big\|\mathbf{g}_k^{full} - \mathbf{g}_{k-1}^{full}\Big\|^2\bigg).$$

□